Available online at www.sciencedirect.com
SCIENCE DIRECT®
Computers & Fluids 35 (2006) 641–669
computers & fluids
www.elsevier.com/locate/compfluid

Review

Residual distribution schemes: Current status and future trends

Rémi Abgrall *

Institut Universitaire de France and Mathématiques Appliquées de Bordeaux, Université Bordeaux I, 33 405 Talence Cedex, France

Received 1 August 2004; accepted 10 January 2005
Available online 10 February 2006

Abstract

In this paper, we discuss a new class of schemes, the residual distribution schemes, adapted to compressible flow problems. They can be seen as a link between pure finite element methods such as the streamline diffusion method and the high order upwind method finite volume schemes. In fact they borrow ideas from both classes and this results in very accurate compact schemes. Up to now, they are mainly adapted to triangular type meshes, but can handle steady and unsteady problems. Since the philosophy is quite different form standard schemes, we will provide a full description of the schemes and many numerical illustrations. Some still unsolved issues will also be discussed.
© 2005 Elsevier Ltd. All rights reserved.

Contents

* Tel.: +33 540 00 60 68; fax: +33 540 00 26 26.
E-mail address: abgrall@math.u-bordeaux.fr

0045-7930/$ - see front matter © 2005 Elsevier Ltd. All rights reserved.
doi:10.1016/j.compfluid.2005.01.007

1. Introduction

We are interested in the numerical approximation of the Euler equations of fluid mechanics in a domain Ω with boundary conditions,

$$\begin{aligned} &\frac{\partial W}{\partial t} + \operatorname{div}\mathscr{F}(W) = 0, \quad t > 0 \text{ and } x \in \Omega \\ &W(x,0) = W_0(x), \quad x \in \Omega \\ &\text{Boundary conditions} \quad \text{on } \partial\Omega \end{aligned} \tag{1}$$

In this paper, we focus on the two-dimensional case only. The three-dimensional case has, of course, already been considered elsewhere. Since the problems and the methods are the same than in the 2D case, and for the sake of simplicity, we have preferred to focus on the lower dimension case.

The flux $\mathscr{F} = (F, G)$ and the conserved variables are given by

$$W = (\rho, \rho u, \rho v, E)^{\mathrm{T}},$$

$$F(W) = (\rho u, \rho u^2 + p, \rho uv, u(E+p))^{\mathrm{T}} \quad \text{and}$$

$$G(W) = (\rho v, \rho uv, \rho v^2 + p, v(E+p))^{\mathrm{T}}$$

where ρ is the density, u and v are the components of the velocity, ϵ the internal energy and $E = \rho\epsilon + \frac{1}{2}\rho(u^2+v^2)$ is the total energy. The system is closed by the equation of state relating the pressure p to the conserved variables,

$$p = (\gamma - 1)\left(E - \frac{1}{2}\rho(u^2+v^2)\right) = (\gamma-1)\rho\epsilon.$$

In the following the matrix $A = A(W)$ (respectively $B = B(W)$) is the Jacobian matrix $\nabla_W F$ (respectively $\nabla_W G$) evaluated at the state W. Last, the ratio of specific heats γ is kept constant, $\gamma = 1.4$ in the applications.

The system (1) has to be supplemented by the entropy inequality which translates the second law of thermodynamics,

$$\frac{\partial S}{\partial t} + \frac{\partial (uS)}{\partial x} + \frac{\partial (vS)}{\partial y} \leqslant 0 \text{ on } \Omega. \tag{2}$$

Here, the mathematical entropy is given by $S = -\rho h(s)$ [1], where s is the physical entropy

$$s = c_v \log\left(\frac{p}{\rho^\gamma}\right) + s_0 \tag{3}$$

and h is any real valued function such that

$$h' > 0 \quad \text{and} \quad \frac{h''}{h'} < \gamma^{-1}.$$

In the practical examples, we take $h(x) = x$. If the flow is smooth, (3) is equivalent to

$$\frac{\partial s}{\partial t} + u\frac{\partial s}{\partial x} + v\frac{\partial s}{\partial y} = 0 \quad (\geqslant 0) \tag{4}$$

and E. Tadmor has shown [2] that the solution (if it is bounded) enjoys the following minimum principle

$$s(x,t) \geqslant \min_{\|y-x\| \leqslant t\|\vec{u}\|_\infty} s(y,0), \tag{5}$$

where $\|x\|$ is the Euclidean norm of x and $\|\vec{u}\|_\infty$ is the L^∞ norm of the velocity field.

For introducing and analysing in some details the residual distributive schemes (RD for short), we often rely on a scalar version of (1), the transport equation

$$\frac{\partial u}{\partial t} + \mathbf{a}\cdot\nabla u = 0. \tag{6}$$

This equation is supplemented by Dirichlet boundary conditions on the inflow part Γ^- of the computational domain Ω that, denoting by $\mathbf{n}(x)$ the unit normal vector to $\partial\Omega$ at $x \in \partial\Omega$, is defined by

$$\Gamma^- = \{x \in \partial\Omega,\ \mathbf{n}(x)\cdot\mathbf{a} \leqslant 0\}$$

and also by initial conditions. The steady version of (6) is

$$\begin{aligned} &\mathbf{a}\cdot\nabla u = 0 \quad x \in \Omega, \\ &u = g \qquad\ x \in \Gamma^-. \end{aligned} \tag{7}$$

In some applications, we need the nonlinear version of (6) and (7), namely

$$\frac{\partial u}{\partial t} + \operatorname{div}\mathbf{f}(u) = 0, \tag{8}$$

supplemented by initial and boundary conditions, and its steady version

$$\begin{aligned} &\operatorname{div}\mathbf{f}(u) = 0 \quad x \in \Omega, \\ &u = g \quad x \in \Gamma^-. \end{aligned} \tag{9}$$

In (8) and (9), the flux $\mathbf{f} = (f, g)$ is continuously differentiable with respect to u.

Computing the solutions of (1) has become a routine task in many modern CFD codes. Many current schemes use the ideas developed in the 70–80's for high resolution schemes by van Leer, Roe, Osher, Harten, Yee, Sweby, and many others. The list is enormous, and some of the most significant contributions has been collected in [3]. However, the quality of the solution is still questionable: some apparently simple problems such as computing the lift and drag of an airfoil is still a difficult task. One of the reasons is that the so-called high resolution schemes suffer a much too important entropy production. In fact, they have been devised on scalar 1D problems, then extended to multiD systems but their construction relies on "1D ideas". Another difficult problem is the sensitivity to the mesh: It is still difficult to construct 3D mesh with a very good quality and consequently, the quality of the solution itself may be questionable in many cases. Hence, it is natural to try to develop methods that are as little as possible sensitive to the regularity of the mesh.

For these reasons, since several years, some researchers have tried to incorporate some ideas contained in the 1D high resolution schemes (upwinding and monotonicity preservation) in a finite element like framework. Some of the major contributions has been done by Roe, Deconinck, Sidilkover and their coauthors. These residual distribution (or fluctuation splitting) schemes have first been developed for a scalar transport equation, then formally extended to the system (see [4,5] for example) by incorporating as much physics as possible. These schemes share common features with the SUPG scheme of Hughes or the streamline diffusion methods of Johnson, except for upwinding. These schemes are not constructed by using any particular direction of the mesh. One of their advantage is that, at least for scalar equations, one can construct a fully second order accurate scheme on triangular meshes with a very compact stencil: the scheme uses only the neighboring nodes. In the finite difference context, it is interesting to note the paper by Ni [6] which is the first, up to our knowledge, where the idea of splitting an elementwise quantity was splitted in part to update the solution, and also the work by Lerat and coworker that share many similarities with the SUPG-like scheme, [7–9].

The upwind residual distribution schemes have first been imagined by Roe in [10] and then in collaboration with Deconinck and collaborators. The status of this work have been reported in a series of von Karmàn Institute Lecture Series in the 90's, one example is [4], or a series or PhD thesis such as Paillère's [11] or van der Weide's [12]. Later contributions are [13] or [14–18]. The 2002 state-of-the-art is reported in a special issue of *Computer and Fluids* [19] and in the 33rd Lecture series of the von Karmàn Institute [20–22].

This paper is organised as follows. We first give some generalities on residual distribution schemes. In particular, we connect them to finite volume schemes and show why they offer more flexibility. We recall Roe–Struijs–Deconinck linearisation [23] give a simple condition that guarantees a Lax Wendroff like theorem and describe the design principle of our scheme. Then, we recall two important examples of the system N (narrow) and the LDA (low diffusion advection) system schemes introduced by van der Weide and Deconinck [24] after their scalar version. We show that they are well defined for a symmetrizable system. Barth [25,15] has shown that for a linear symmetrizable system the N scheme is globally and locally dissipative. In a next section, we give a different interpretation of the PSI scheme, and we show how to extend it to (1). The extension to viscous problems is discussed. Numerical examples are given to illustrate the scheme. All this material is provided in Section 2. Then, following the same lines, we consider unsteady problems in the scalar and system case in Section 3. In Section 4 we discuss what we consider to be the most important problems to solve for RD scheme, namely the problem of erratic convergence in some situations and the high order extension of the RD scheme (i.e. higher than second order accuracy), and then conclude.

2. Residual distribution for steady problems

In this section, we are interested in the steady problem (1). We consider a conformal mesh which elements are triangles in 2D and tetrahedrons in 3D. In all what follows, in order to make the notations simpler we assume to work in two dimensions, but everything can be easily extended to 3D. The triangles are denoted by $\{T_l\}_{l=1,\dots,n_t}$, n_t is the number of elements. The vertices are denoted by $\{M_i\}_{i=1,\dots,n_s}$, n_s the number of vertices. We denote by M_{j_1}, M_{j_2} and M_{j_3} the three vertices of T. In most cases, there is no ambiguity, so these vertices are simply denoted by M_1, M_2 and M_3, or 1, 2, 3. In all what follows, we assume that the mesh is regular. We also denote by h the maximum of the diameters of the triangles.

2.1. Generalities

In the RD schemes, the data are stored at vertices. Hence, W_i is an approximation of $W(M_i)$. Eq. (1) is then approximated by

$$\sum_{T, M_i \in T} \Phi_i^{\mathrm{T}} = 0. \tag{10}$$

The quantities Φ_i^{T} are called residual. In general, they depend on W_j where $j \in \mathscr{V}(i)$ a finite set of indices. They have to fulfill the conservation relation

$$\sum_{M_i \in T} \Phi_i^{\mathrm{T}} = \int_T \operatorname{div}(F(W))^h \,\mathrm{d}x := \Phi^{\mathrm{T}}, \tag{11}$$

where $(F(W))^h$ is an approximation of the continuous flux F. The system (10) is never solved as it appears, but via an iterative procedure. One simple example is given by

$$W_i^{n+1} = W_i^n - \frac{\Delta t}{|C_i|} \sum_{T, M_i \in T} \Phi_i^{\mathrm{T}}, \tag{12}$$

where we seek for the limit, when $n \to +\infty$, of W_i^n. The parameter Δt can be interpreted as a pseudo-time step, while $|C_i|$ is the area of the dual control volume. In other words, we seek for an approximation of the unsteady Euler equation when the time goes to infinity. Obviously, local time stepping can be used, in which case the iterative method is interpreted as a relaxation method of the Jacobi type. Last, the boundary conditions are enforced weakly, see [14] for an example of technique.

2.2. Accuracy, monotonicity and conservation issues

In this section, we provide some design features of the schemes. Ideally, they should be monotone, stable, accurate, convergent, etc. Here we provide simple conditions to ensure the monotonicity, accuracy, and simple criteria that garanties they converge to a solution of the problem, provided the numerical sequence does converge.

2.2.1. Monotonicity preserving schemes, scalar case

In practice, all the known RD schemes can be written as

$$\Phi_i^{\mathrm{T}} = \sum_{M_j \in T, M_i \neq M_i} c_{ij}^{\mathrm{T}} (u_i - u_j). \tag{13}$$

For this scheme to be L^∞ stable, it is enough that

$$c_{ij}^{\mathrm{T}} \geqslant 0 \quad \text{for all } i, j. \tag{14}$$

The method is monotone, and the iterative method (12)

$$u_i^{n+1} = u_i^n - \frac{\Delta t_i}{|C_i|} \sum_{T, M_i \in T} \Phi_i^{\mathrm{T}}$$

is monotone under the CFL-like condition

$$\Delta t_i \max_{T, i \in T} \left(\frac{\sum_{j \in T} c_{ij}^{\mathrm{T}}}{|T|} \right) \leqslant 1.$$

The condition (14) is the so-called monotonicity preserving condition.

2.2.2. Accuracy: the linear preserving (LP) condition

We briefly recall the analysis of [14]. It is shown that a *converged* RD scheme (10) produces a formally second order accurate solution of the *steady problem* (1) under the following three requirements:

1. The mesh is regular,
2. The approximation F^h is second order accurate on smooth solutions,
3. For any smooth solution of (1), $\Phi_i^{\mathrm{T}}(W) = \mathcal{O}(h^3)$ for any vertex M_i and any triangle T such that $M_i \in T$.

For this reason, it is *essential* that Eq. (10) is exact or approximately exact with an error at most $\mathcal{O}(h^3)$ otherwise accuracy is lost.

In most cases, the third condition is met by imposing that there exists a family of uniformly bounded coefficients (or matrices for system problems) β_i^{T} such that

$$\Phi_i^{\mathrm{T}} = \beta_i^{\mathrm{T}} \Phi^{\mathrm{T}}.$$

Indeed, it is easy to show that

$$\int_{\partial T} F^h(W^h)\, \mathrm{d}l = \mathcal{O}(h^3),$$

when $F^h(W^h)$ is a second order approximation corresponding to a smooth solution. This is the linearity preservation (LP) condition introduced in [4] which is satisfied by the SUPG scheme and the PSI scheme of Struijs [23] that we recall later.

It is known that it is not possible to have a linear scheme that is both monotonicity preserving and linearity preserving: this is Godunov theorem [26]. The schemes that satisfy both requirements must be nonlinear. The construction of such schemes is the topic of the next section.

2.2.3. Conservation

The conservation relation (11) garanties under rather mild assumptions, that the scheme, if it converges, converges to a weak solution of the problem. More precisely, we temporarily denote by $(W_i^h)_{i=1,\ldots,n_s}$ the solution of (10) to indicate the mesh dependency. In [27], it is shown that under the following conditions:

1. the mesh is regular,
2. the approximation $(F(W))^h$ is continuous across the edges of the triangles T,
3. when the mesh size converges to 0, $(F(W))^h \to F(W)$ in a suitable norm (L^1_{loc} or L^2_{loc}),
4. the functions $\Phi_i^{\mathrm{T}} = \Phi_i^{\mathrm{T}}(W_j, j \in \mathscr{V}(i))$ is continuous,
5. the conservation condition (11) is satisfied,
6. the solution $(W_i^h)_{i=1,\ldots,n_s}$ is bounded in the maximum norm when the mesh size $h \to 0$ and there exists a locally square integrable function W such that a subsequence of $(W_i^h)_{i=1,\ldots,n_s}$ converges to W in $L^2(\Omega)$,

then W is a weak solution of (1).

Hence, the conservation relation (11) is essential for the quality of the solution. What about nonlinear problems like (1) or (9)? Most of the schemes are first constructed for a linear problem and not for nonlinear ones. So, one has to find a linearised problem such that its residual on any triangle is equal to the residual (11). This is, in general, a nontrivial question, except when the flux depends quadratically of the conserved variable.

Consider for example the case of the Burger equation

$$\frac{\partial u}{\partial y} + \frac{1}{2} \frac{\partial u^2}{\partial x} = 0. \tag{15}$$

The only thing we know how to do is to construct RD scheme for a linear advection problem,

$$\mathbf{a}_x \frac{\partial u}{\partial x} + \mathbf{a}_y \frac{\partial u}{\partial y} = 0, \tag{16}$$

that is to construct residuals Φ_i such that

$$\Phi_1 + \Phi_2 + \Phi_3 = \Phi = \int_T \left(\mathbf{a}_x \frac{\partial u^h}{\partial x} + \mathbf{a}_y \frac{\partial u^h}{\partial y} \right) \mathrm{d}x\,\mathrm{d}y,$$

where we have assumed a piecewise linear interpolation. How can we construct $(\mathbf{a}_x, \mathbf{a}_y)$ such that conservation holds for (15), i.e.

$$\int_T \left(\mathbf{a}_x \frac{\partial u^h}{\partial x} + \mathbf{a}_y \frac{\partial u^h}{\partial y} \right) \mathrm{d}x\,\mathrm{d}y = \int_T \left(\frac{\partial u^h}{\partial y} + \frac{1}{2} \frac{\partial (u^h)^2}{\partial x} \right) \mathrm{d}x\,\mathrm{d}y.$$

The answer is obtained via a Roe type linearisation since the fluxes are quadratic,

$$\mathbf{a}_x = 1 \quad \text{and} \quad \mathbf{a}_y = \frac{u_1 + u_2 + u_3}{3}.$$

In the system case, the answer is the similar, see [26]. In particular, in the case of the Euler equation with a *constant* polytropic coefficient γ, it is known that the Roe parameter vector

$$Z = \sqrt{\rho}(1, u, v, H)^{\mathrm{T}}$$

permits to write the fluxes $F := F(Z)$ and $G := G(Z)$ quadraticaly in Z, as well as the conserved variable $W := W(Z)$. Then, it is possible to construct averaged Jacobians $\overline{A}$ and $\overline{B}$ such that

$$\int_T \mathrm{div} F^h(W^h)\,\mathrm{d}x = \overline{A} \int_T \frac{\partial W^h}{\partial x}\,\mathrm{d}x + \overline{B} \int_T \frac{\partial W^h}{\partial y}\,\mathrm{d}x,$$

where it is understood that $F^h(W^h) := F(Z^h)$, $W^h := W(Z^h)$ and Z^h is the linear interpolant of Z in T. The interesting point is that the system

$$\frac{\partial V}{\partial t} + \overline{A} \frac{\partial V}{\partial x} + \overline{B} \frac{\partial V}{\partial y} = 0 \tag{17}$$

is also hyperbolic for a constant γ, see for example [14] for details. This is some sort of a coincidence, because the hyperbolicity of (17) has nothing to do with the way it was constructed.

There are several important differences with the one-dimensional situation. In one dimension, there are several ways of deriving the Roe linearisation. One is the use of the Roe parameter vector, another one is to write explicitly the relation

$$\overline{A} \Delta W = \Delta F \tag{18}$$

with $\Delta f := f_L - f_R$ with the choice $\overline{A} = \frac{\partial F}{\partial W}(\overline{W})$ at some average state to be determined and to realise that one has to solve a quadratic equation in $\bar{u}$ and a linear one in $\overline{H}$ to get the result. The quadratic relation has two solutions

$$\bar{u}_1 = \frac{\sqrt{\rho_L} u_L + \sqrt{\rho_R} u_R}{\sqrt{\rho_L} + \sqrt{\rho_R}}, \quad \bar{u}_2 = \frac{\sqrt{\rho_L} u_L - \sqrt{\rho_R} u_R}{\sqrt{\rho_L} - \sqrt{\rho_R}} \tag{19}$$

and only one stays bounded whatever the density values: the Roe average of the velocity.

Another method is that the difference operator $\Delta f := f_L - f_R$ that defines the difference of a function f between two states f_L and f_R has the same properties as a derivation. It is known that if f and g are two real valued functions, then the derivative $(fg)'$ is

$$(fg)' = f'g + fg'.$$

Similarly, for any $\lambda \in [0, 1]$ one has

$$\Delta(fg) = \bar{g}\Delta f + \underline{f}\Delta g, \tag{20}$$

where $\bar{f} = \lambda f_L + (1 - \lambda) f_R$ and $\underline{g} = (1 - \lambda) g_L + \lambda g_R$. Thanks to this relation and the choice

$$\lambda = \frac{\sqrt{\rho_L}}{\sqrt{\rho_R} + \sqrt{\rho_L}},$$

one gets the Roe average.

In two dimensions, the situation is very different. The method starting form (18) can be generalised. Instead of two generic solutions (19), one has in general four solutions, among which only one remains bounded what ever the density values. Unfortunately, it is very difficult to compute in general and, last but not least, the linearised system (17) may not be hyperbolic. Thus this of no use, see [28,29] for details. The second method cannot be extended to the RD case since the algebraic relation (20) cannot be generalised in several dimensions, so that no "formal" derivation relation seems to exist. The only solution is the use of the Roe parameter vector, but it works only for ideal gases ...Some solutions to overcome the problem have been proposed, see [15,30], the most promission is [30].

This situation is in contrast with what can be done for finite volume schemes. Here, it is sufficient to define a continuous numerical flux $\mathscr{F}$ that satisfies

$$\mathscr{F}(W_i, W_j, \vec{n}_{ij}) = -\mathscr{F}(W_j, W_i, \vec{n}_{ji})$$

to ensure conservation in the general case, see [31,32]. In the RD scheme, one has to establish a global conservation relation at the level of the triangle T, which is much more difficult. We show in Section 4.2 that in fact, when going to high order schemes, the situation becomes surprisingly much easier, so that conservation is not any more a problem.

2.3. First examples

Many very classical schemes can be formulated within the framework of RD schemes. An example is given by the finite volume schemes, see [14]. In that case, and whatever the order of accuracy of the scheme, the approximation $(F(W))^h$ is defined in each triangle T as the Lagrange interpolation of the flux F. If $\mathscr{N}_i$ is the piecewise linear shape function associated to the vertex M_i, the restriction of $(F(W))^h$ in T is

$$(F(W))^h = \sum_{i \in T} F(W_i) \mathscr{N}_i.$$

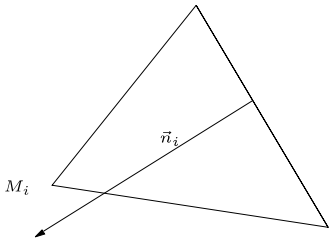

Fig. 1. Definition of is the inward normal vector opposite to the vertex M_i.

In that case, we have

$$\Phi^{\mathrm{T}} = \frac{1}{2}\sum_{j\in T} F(W_j)\cdot\vec{n}_i,$$

where $\vec{n}_i$ is the inward normal vector opposite to the vertex M_i, see Fig. 1 for the notations.

However, the schemes defined by (10) and (11), where $(F(W))^h$ satisfy the above conditions, represent a much wider class than the finite volume ones. In particular, the finite volume are constructed using directions that are only related to the mesh definition, not the structure of the solution. Other schemes, that also satisfy (10) and (11), can be defined without any reference to the geometry of a control volume and by using more deaply the physical structure of the local flow.

Among the schemes that cast into the formalism (10) and (11) are the streamline diffusion method of Johnson et al. [33] and the SUPG scheme of Hughes et al. [34]. We denote by W^h the continuous piecewise linear interpolant of $(W_i^h)_{i=1,\dots,n_s}$ and let V^h any continuous piecewise linear test function. These schemes writes for (1)

$$\text{for all } V^h,\quad \int_\Omega V^h\cdot \mathrm{div} F(W^h)\mathrm{d}x + \sum_{T\subset\Omega} h_T\int_T (\nabla_W F(W^h)\cdot\nabla V^h)(\nabla_W F(W^h)\cdot\nabla W^h)\,\mathrm{d}x = 0.$$

In that case, the residual writes

$$\Phi_i^{\mathrm{T}} = \int_T \mathscr{N}_i\cdot \mathrm{div}\ F(W^h)\,\mathrm{d}x + h_T\int_T (\nabla_W F(W^h)\cdot\nabla\mathscr{N}_i)\times(\nabla_W F(W^h)\cdot\nabla W^h)\,\mathrm{d}x.$$

The last example of this type we provide in this section is an extension of the Lax Friedrichs scheme. The residual is

$$\Phi_i^{\mathrm{T}} = \frac{1}{3}\left(\Phi^{\mathrm{T}} - \alpha_T\sum_{j\in T, j\neq i}(W_i - W_j)\right). \tag{21}$$

Clearly, $\Phi_1^{\mathrm{T}} + \Phi_2^{\mathrm{T}} + \Phi_3^{\mathrm{T}} = \Phi^{\mathrm{T}}$. The parameter α is chosen larger than the spectral radius of A and B. If the approximation $(F(W))^h$ in (11) is the linear interpolation of the flux, this is the RD formulation of the finite volume Lax Friedrichs scheme. If another approximation is chosen, as the one using the Roe parameter vector [26], this leads to non finite volume scheme, i.e., no numerical flux associated with precise directions in the mesh seems to be related to that scheme.

2.4. Upwind residual distribution schemes

We first recall the construction of these schemes for the linear scalar problem

We consider the problem

$$\begin{aligned} &\mathbf{a}\cdot\nabla u = 0 \quad x\in\Omega,\\ &u = g \quad \text{on } \Gamma_-\end{aligned} \tag{22}$$

where Γ_- is the inflow boundary of $\Gamma = \partial\Omega$. If the unknown u is piecewise linearly interpolated, the total residual Φ^{T} is given by

$$\Phi^{\mathrm{T}} = \sum_{j=1}^{3} k_j u_j,$$

where

$$k_j = \frac{1}{2}\mathbf{a}\cdot\vec{n}_j = \int_T \mathbf{a}\cdot\nabla\mathscr{N}_i\,\mathrm{d}x.$$

We notice that $\sum_{j=1}^3 k_j = 0$. Here, we drop the superscript T in $\Phi_i^{\mathrm{T}}\equiv\Phi_i$ because there is no ambiguity.

We briefly describe the N (narrow) scheme [26]. It writes

$$\Phi_i = k_i^+(u_i - \tilde{u}), \tag{23}$$

where $\tilde{u}$ is obtained by recovering the conservation, i.e.

$$\tilde{u} = \left(\sum_j k_j^-\right)^{-1}\left(\sum_j k_j^- u_j\right). \tag{24}$$

In (23), we have set as usually $k_i^+ = \max(k_i, 0)$ and $k_i^- = \min(k_i, 0)$ so that $k_i = k_{i1}^+ + k_i^-$.

The scalar $n := \left(\sum_j k_j^-\right)$ is always defined unless $\mathbf{a} = 0$.[1] This scheme can be considered as a conservative method of characteristics.

There are two possible types of triangles, the one target triangles and the two targets triangles, see Fig. 2. In fact, since $\sum_{j=1}^3 k_j = 0$, either one of the k_js is positive and the others are all negative: this is the one target case, or two k_js are positive and the last is negative: this is the two target case.

- *One target case*. We assume $k_1 > 0$ and $k_2, k_3 \leqslant 0$. Then, $\Phi_1 = \Phi$, and $\Phi_2 = \Phi_3 = 0$.
- *Two targets case*. We assume $k_1 \geqslant 0$ and $k_2 \geqslant 0$, so $k_3 \leqslant 0$. Thus, $\Phi_3 = 0$, and simple calculations lead to

$$\Phi_1 = k_1(u_1 - u_3),$$
$$\Phi_2 = k_2(u_2 - u_3).$$

[1] Since for any i, $\Phi_i \to 0$ uniformly if $\mathbf{a}\to 0$, there is no definition problem in the case $\mathbf{a} = 0$.

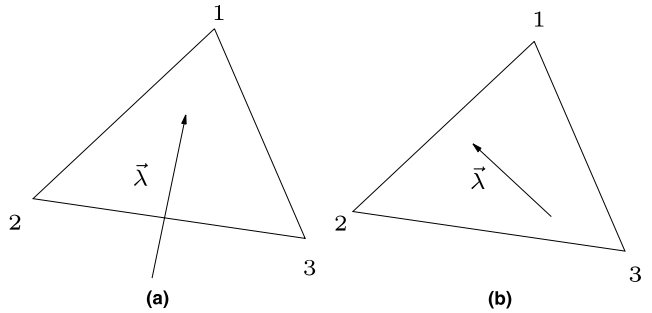

Fig. 2. One target and two target cases for the N and LDA schemes.

The relations (23) and (24) ensure a continuous switch between the one target case and the two target case. Note that any interior node is always one target with respect to exactly one of the triangles that surround it. This feature seems to have an important role in the good behavior of the N scheme and of its high order counterparts.

Eq. (23) can be rewritten as

$$\Phi_i = \sum_{j\in T, j\neq i} c_{ij}^{\mathrm{T}}(u_i - u_j)$$

with $c_{ij}^{\mathrm{T}} = k_i^+ n k_j^- \geqslant 0$. Because of that, the method is monotone, and the iterative method (12)

$$u_i^{n+1} = u_i^n - \frac{\Delta t_i}{|C_i|}\sum_{T, M_i\in T}\Phi_i^{\mathrm{T}}$$

is monotone under the CFL-like condition

$$\Delta t_i \max_{T, i\in T}\left(\frac{k_i^+}{|T|}\right) \leqslant 1.$$

Another upwind scheme is the LDA scheme (for low diffusion advection), see [4]. It is defined as

$$\Phi_i = -nk_i^+\Phi.$$

This is an upwind scheme, it is not monotone. Note that the LDA scheme is identical to the N scheme for one target triangles. The main difference between the two schemes, besides the monotony problem, is accuracy for *steady* problems. The N scheme is only first order, since in general the ratio $\frac{\Phi_i}{\Phi}$ are not uniformly bounded. The LDA scheme is linear preserving since these ratio are equal to $-nk_i^+$ and lies in $[0,1]$. If the N scheme provides nonoscillatory solutions, the LDA will be oscillatory, but only near discontinuities.

2.5. Construction of LP, monotony preserving second order schemes

The problem is the following. Considering a triangle T, we are given residuals that define a first order monotone scheme, (Φ_1, Φ_2, Φ_3). More precisely, we demand that it satisfies the local monotonicity conditions (14). We want to construct a second order scheme defined by its residuals $(\Phi_1^*, \Phi_2^*, \Phi_3^*)$ such that the resulting scheme is still locally monotonicity preserving under a CFL type conditions, is also linear preserving and satisfies

$$\sum_{i=1}^3 \Phi_i = \sum_{i=1}^3 \Phi_i^* = \Phi.$$

The first remark is that if one defines $x_i = \frac{\Phi_i}{\Phi}$, we notice that

$$\sum_{i=1}^3 x_i = 1.$$

Then we define $\beta_i = \frac{\Phi_i^*}{\Phi}$, the problem can be reformulated as finding a mapping $(x_1, x_2, x_3) \mapsto (\beta_1, \beta_2, \beta_3)$ such that

1. Conservation $\sum_{i=1}^3 \beta_i = 1$.
2. Monotonicity: for all $i = 1, 2, 3$, $x_i\beta_i \geqslant 0$. Using (13) and (14), this condition comes from the fact that
$$\Phi_i^* = \frac{\Phi_i^*}{\Phi}\frac{\Phi}{\Phi_i}\Phi_i = \frac{\beta_i}{x_i}\sum_{j\neq i} c_{ij}(u_i - u_j) = \sum\nolimits_{j\neq i} c_{ij}^*(u_i - u_j)$$
with $c_{ij}^* = \frac{\beta_i}{x_i}c_{ij}$. Since $c_{ij} \geqslant 0$, the positivity of c_{ij}^* is equivalent to $x_i\beta_i \geqslant 0$.
3. Linear preserving condition: we want β_i bounded for any i.

In [35], we provide a geometrical interpretations of these conditions, and several solutions to this problem. We repeat the argument. The key remark is that since $\sum_j x_j = \sum_j \beta_j = 1$, we can interpret the coordinates (x_1, x_2, x_3) and $(\beta_1, \beta_2, \beta_3)$ as the barycentric coordinates of points L and H with respect to a reference triangle (A_1, A_2, A_3) that we choose to be equilateral for symmetry. The points L and H are defined by

$$L = x_1A_1 + x_2A_2 + x_3A_3 \quad \text{or equivalently}$$
$$\vec{A_1L} = x_2\vec{A_1A_2} + x_3\vec{A_1A_3},$$
$$H = \beta_1A_1 + \beta_2A_2 + \beta_3A_3 \quad \text{or equivalently}$$
$$\vec{A_1H} = \beta_2\vec{A_1A_2} + \beta_3\vec{A_1A_3}.$$

In Fig. 3(a), we have defined seven sub-domains: the triangle (A_1, A_2, A_3) and the six domains D_i. The problem is to find a mapping that project the point L onto the triangle (A_1, A_2, A_3) so that L and H belongs to the same subdomain. A geometrical representation of a possible projection is given in Fig. 3(b). Note that here, the projection leaves invariant the triangle T. What is important is that the coefficients β_j be bounded, so any bounded region can play the role of invariant region onto which the projection is carried out, for example the disk $\mathscr{D}$ of Fig. 3(b).

One of these possible projections is the PSI "limiter"

$$\beta_i = \frac{x_i^+}{\sum_j x_j^+}, \tag{25}$$

so that

$$\Phi_i^* = \beta_i\Phi. \tag{26}$$

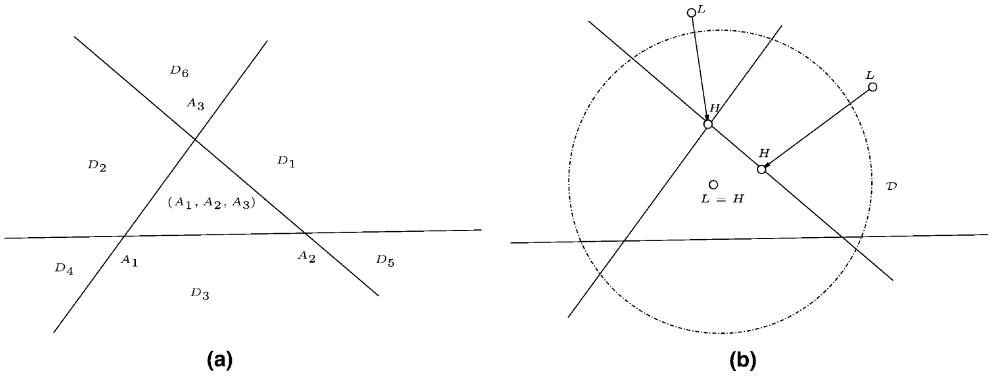

Fig. 3. Geometrical representation of the mapping $(x_1, x_2, x_3) \mapsto (\beta_1, \beta_2, \beta_3)$.

We note that there is no difficulty in the definition of β_i (except the fact that Φ may vanish, in which case we set $\Phi_i^* = 0$) because

$$\sum_j x_j^+ = \sum_j x_j - \sum_j x_j^- \geqslant \sum_j x_j = 1.$$

This construction can be applied to *any* monotone scheme, for example the N scheme, or any finite volume scheme. When applied to the N scheme, this results into the PSI scheme of Struijs which was the first monotone, LP scheme in the literature.

We provide some examples on the Burger equation (15) in $\Omega = [0,1] \times [0,1]$ with the boundary conditions

$$u(x,y) = \begin{cases} 1.5 & \text{if } x = 0, \\ 1.5 - 2x & \text{if } y = 0, \\ -0.5 & \text{if } x = 1 \end{cases} \tag{27}$$

by the N scheme, the PSI scheme, the upwind finite volume scheme and its PSI version, the Lax Friedrichs scheme and its PSI modification in Fig. 5, the mesh is displayed in Fig. 4. As a reference, we provide the results of a second order ENO scheme on the same problem, in Fig. 6. The first remark is that the general quality of the RD solutions is better than that of the ENO scheme. This is particularly true in the resolution of the discontinuity. The second remark is that there is a very clear improvement of the solution between the first order ones and the second order modification of each RD scheme. This is particularly true for the Lax Friedrichs scheme. The third remark is that

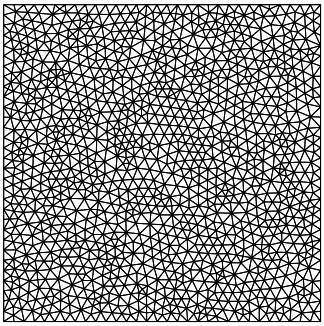

Fig. 4. Mesh for the scalar problem (15)–(27).

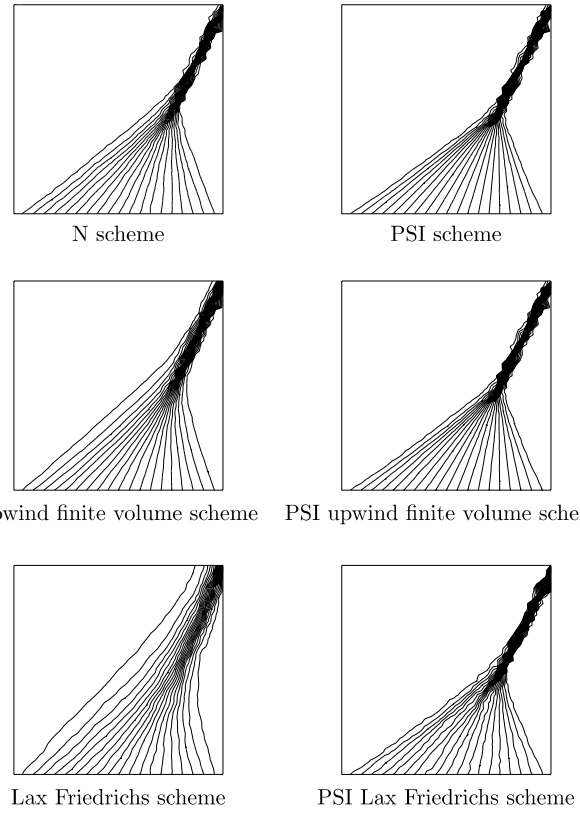

Fig. 5. Results for the problem (15)–(27).

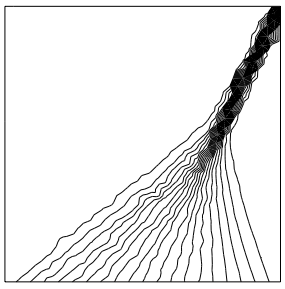

Fig. 6. Solution for the second order ENO scheme of [28]. This scheme has been measured to be second order accurate for smooth solutions. However, the ENO schemes are not particularly tuned for steady problems.

there is a ranking in the solutions. The best first order scheme is the N one, followed by the upwind finite volume scheme and then the Lax Friedrichs one. The same ranking applies for the second order scheme, the PSI scheme being the best, and the PSI upwind finite volume giving almost identical results. The interesting thing is the occurrence of wiggles in the smooth part of the solution provided by the PSI Lax Friedrichs solution. It is interesting to notice that in general, difficulties for the RD schemes occur not in the discontinuities of the solutions (as usually), but in their smooth parts. Coming back to the PSI Lax Friedrichs, these wiggles are not an indication of any instability: the scheme is perfectly stable, the results are converged, and any cut through the fan show that the solution preserves indeed the monotony! The reason of that phenomena is not clear at all. We believe that it is an indication of the overcompressive nature of the limiter, the way to avoid this is not yet understood and is a topic of current research. More generally speaking, the monotonicity condition (14) only ensures that on has, for any vertex i,

$$\min_{j\in\mathcal{V}(i)} u_j \leqslant u_i \leqslant \max_{j\in\mathcal{V}(i)} u_j. \tag{28}$$

It does not tell anything on the behavior of the solution, and indeed, an oscillatory behavior is not in compatible with the inequalities (28). In [36], Breuss shows that even in one dimension, the Lax Friedrichs scheme may produce oscillatory solutions: the solution is oscillatory, but its total variation is not increased.

2.6. Extension to systems

We sketch the work that has been done in [17]. Related work, in a different spirit, has also be done in [12] and is also available in [37] and described in more details in [20]. Another method is described in [14].

2.6.1. The system N scheme

In [17], we have considered only the case of the system N scheme, and provided a method similar to what is done in the scalar case to rise the order of accuracy from first to second order, for steady problems. The system N scheme has been derived in [12,24] and analysed in part in [15] and then in [17].

Similarly to the scalar case, it writes for a linear hyperbolic system with constant matrices A and B as

$$\Phi_i = K_i^+(W_i - \widetilde{W}),$$

where, if n_x^i (respectively n_y^i) are the x- (respectively y-) components of $\vec{n}_i$, we set $K_i = n_x^i A + n_y^i B$. The matrix K_i^+ has the same eigenvectors than K_i, its eigenvalues being the positive parts of those of K_i. Similarly, we define K_i^- so that $K_i = K_i^+ + K_i^-$ and $|K_i| = K_i^+ - K_i^-$. Last, the state $\widetilde{W}$ is defined using the conservation principle,

$$\widetilde{W} = \left(\sum_j K_j^-\right)^{-1}\left(\sum_j K_j^- W_j\right).$$

In the case of the Euler system (1) where a linearisation is performed, some care has to be done since the linearisation relation do *not* provide

$$\sum_j K_j W_j = \int_T \operatorname{div}\mathbf{F}(W(Z^h))\,\mathrm{d}x.$$

Let $Z = (z_1, z_2, z_3, z_4)$ be the Roe's parameter vector and let us write

$$W = \frac{1}{2}D(Z)Z, \qquad \mathbf{F}(W) = \frac{1}{2}\mathbf{R}(Z)Z,$$

where $D(Z)$ is linear in Z, as well as $\mathbf{R}(Z) = (R_x(Z), R_y(Z))$. There are many possible choice, we choose the one that ensures $D(Z)Z' = D(Z')Z$ and $\mathbf{R}(Z)Z' = (Z')Z$. For example,

$$D(Z) = \begin{pmatrix} z_1 & 0 & 0 & 0 \\ z_2 & z_1 & 0 & 0 \\ z_3 & 0 & z_1 & 0 \\ \frac{z_4}{2\gamma} & \frac{(\gamma-1)}{2\gamma}z_2 & \frac{(\gamma-1)}{2\gamma}z_3 & \frac{z_1}{2\gamma} \end{pmatrix}.$$

Then, the total residual is

$$\begin{aligned}\Phi &= \int_T \operatorname{div}\mathbf{F}(W(Z^h))\,\mathrm{d}x = \int_T \mathbf{R}(Z^h)\nabla Z^h\,\mathrm{d}x \\ &= \frac{1}{2}\mathbf{R}(Z_1)\cdot\vec{n}_1 Z_1 + \frac{1}{2}\mathbf{R}(Z_2)\cdot\vec{n}_1 Z_2 + \frac{1}{2}\mathbf{R}(Z_3)\cdot\vec{n}_1 Z_3 \\ &= K_1 D^{-1}(\overline{Z})Z_1 + K_2 D^{-1}(\overline{Z})Z_2 + K_3 D^{-1}(\overline{Z})Z_3 \\ &= K_1\widehat{W}_1 + K_2\widehat{W}_2 + K_3\widehat{W}_3.\end{aligned}$$

In the above equation, we have made the convention that $\mathbf{R}(Z)\cdot\vec{n} = R_x(Z)n_x + R_y(Z)n_y$.

The parameter vector $\overline{Z}$ is the arithmetic average of the Z_js and $\widehat{W} = D^{-1}(\overline{Z})Z_j$. This shows that the correct evaluation of the residual is

$$\Phi = K_1\widehat{W}_1 + K_2\widehat{W}_2 + K_3\widehat{W}_3,$$

so that the system N scheme, in the case of the linearised Euler equation, writes

$$\Phi_i = K_i^+(\widehat{W}_i - \widetilde{W})$$

with

$$\widetilde{W} = \left(\sum_j K_j^-\right)^{-1}\left(\sum_j K_j^-\widehat{W}_j\right).$$

The evaluation of $\widetilde{W}$ needs to solve a linear system. One can show that this linear system is always solvable in the case of a symmetrizable system, as is the Euler system, see [14] for details. In [15], it is shown that the system N scheme, applied to a constant symmetrisable system is energy stable. In the same reference, it is also shown that under the assumptions of the Lax Wendroff theorem, the system N scheme, for the nonlinear Euler equation, is entropy stable in the limit of a mesh refinement.

2.6.2. Construction of a LP and stable scheme for symmetrisable systems

The idea in [17] is the following. We consider a symmetrizable system, for example the Euler equations. Consider any triangle T, and Let $\{r_\xi\}_\xi$ be the set of eigenvectors of the matrix $\cos\theta_T A + \sin\theta_T B$, for a fixed *arbitrary* angle θ_T. In the case of the Euler equations, one of the eigenvectors do not depend on θ_T: the eigenvector associated to the transport of entropy. It is the only common eigenvector of the matrices A and B. we denote by $\{\ell_\xi\}_\xi$ the set of left eigenvectors of $\cos\theta_T A + \sin\theta_T B$, namely

$$\ell_0 = \begin{pmatrix} 1 \\ u \\ v \\ \frac{u^2+v^2}{2} \end{pmatrix}, \quad \ell_1 = \begin{pmatrix} 1 \\ u - c\cos\theta_T \\ v - c\sin\theta_T \\ H - (\cos\theta_T u + \sin\theta_T v)c \end{pmatrix},$$

$$\ell_2 = \begin{pmatrix} 1 \\ u + c\cos\theta_T \\ v + c\sin\theta_T \\ H + (\cos\theta_T u + \sin\theta_T v)c \end{pmatrix},$$

$$\ell_3 = \begin{pmatrix} 0 \\ -\sin\theta_T \\ \cos\theta_T \\ -u\cos\theta_T + v\sin\theta_T \end{pmatrix}.$$

The next step is to project the residuals of the N scheme against the left eigenvectors of $\cos\theta_T A + \sin\theta_T B$. We set

$$\varphi_i^\xi = \ell_\xi^{\mathrm{T}} \Phi_i$$

and notice that

$$\sum_j \varphi_j^\xi = \ell_\xi^{\mathrm{T}} \Phi := \varphi^\xi.$$

Then, for any $\xi = 0, \ldots, 3$, we limit the set $\{\varphi_i^\xi\}_{i=1,3}$ with any limiter introduced in Section 2.5, for example (25). The limited projected residuals are denoted by $\{\varphi_i^{\xi,*}\}_{i=1,3}$ according to (26). Then we reconstruct residuals for the system case according to

$$\Phi_i^* = \sum_\xi \varphi_i^{\xi,*} r_\xi.$$

The stability of such a procedure is analysed in [17]. In practice, the angle θ_T is that of the flow velocity because it seems more natural, but the stability does not depend on the specific choice of this direction, see [17] for more details.

2.7. Other methods

There exists another technique for achieving second order accuracy, namely the blending technique. Several variants have been illustrated in [14,24,38]. The general idea is to consider the system N scheme and the system LDA scheme and to construct the residual defined by

$$\Phi_i = \ell \Phi_i^N + (\mathrm{Id} - \ell)\Phi_i^{\mathrm{LDA}}.$$

The last step is to construct the family of matrices ℓ such that the scheme is second order accurate at steady state and nonoscillatory. Second order accuracy is achieved if $\ell = \mathcal{O}(h)$ at steady state, following the analysis of Section 2.5.

In [14], the matrix ℓ is constructed so that the entropy production of the scheme within one triangle leads to a (formal) entropy inequality. In [24,38], the blending matrix is constructed componentwise by extending the scalar formula

$$\ell = \frac{|\Phi|}{|\Phi_1^N| + |\Phi_2^N| + |\Phi_3^N|}. \tag{29}$$

It is clear that $0 \leqslant \ell \leqslant 1$, and that in principle $\ell = \mathcal{O}(h)$ for a smooth solution (thus ensuring accuracy), while $\ell = \mathcal{O}(1)$ near a discontinuity, thus ensuring a nonoscillatory behavior. In [14], we show that there exists a family of parameters that ensures the nonoscillatory behavior of the scheme, but the choice (29) does not belong to this family. There exists also a particular choice that enables to recover the scalar PSI scheme of Struijs.

These schemes work very well, and are simple to implement. However, in our opinion, but it is a very subjective opinion, they suffer several drawbacks:

1. They need to compute two residuals for constructing the limited one, instead of only one in the previous construction.
2. The nonoscillatory behavior is only a fact of experience, no proof have yet been given. It is even possible (and difficult) to produce counter examples. In our experiments, difficulties may be encountered for very high Mach number flows.
3. The version of [24,38] is not rotational invariant.
4. We have experimented difficulties in extending this approach (i.e. [14]'s) to nonsteady problems. Deconinck et al. report a better success with their blending approach however, as examples will be given later in the paper.
5. If one imagines to extend this technique to other choices of base schemes, for example the upwind finite volume scheme of Roe instead of the N scheme and the Lax Wendroff scheme instead of the LDA scheme, it is easy to see that in general $\ell = \mathcal{O}(1)$, so that the resulting scheme is only first order accurate, see [17] for details. Such a class of scheme would be interesting since we could construct schemes from classical ones, and reach second order accuracy with the most possible compact stencil, see [39] for details.

The idea of approximating (1) using a balance between element-residual as here, has been used by several authors, such as Hughes et al. [34], Johnson et al. [33] in the finite element context. In the finite difference context, up to our knowledge, the first paper of this type is Ni's paper [6]. A very interesting contribution in the finite difference framework, both for steady and unsteady problems, is Lerat

et al. contribution [7–9]. It shares many similarities with the SUPG approach, especially concerning the type of artificial dissipation they use. However, there are some differences, such as the tuning parameters that are directly related to the wave structure of (1), so that no shock capturing term, at least for transonic problems, seem to be needed.

2.8. Numerical applications

We illustrate the schemes of Section 2.6 on the example of a scramjet-like configuration. The inflow conditions are $M = 3.6$. In this example, we have several strong discontinuities and also interactions between these discontinuities resulting in a quite complex flow. Fig. 7 present the Mach number isolines for the Roe scheme with van Leer–van Albada limiter applied on the physical variables on the right. The results of the PSI scheme for the Mach number are given in Fig. 8. What is noticeable is a sharper resolution of the discontinuities. This can be observed in Fig. 9 where a cross-section on the lower part of the computational domain, parallel to the lower boundary, is given. The important difference between the results obtained by the two schemes can be observed on the zooms of Figs. 7 and 8. Besides the sharpness of the discontinuities, we observe some "oscillations" in the smooth part of the PSI results. Once more this is not a signal of instability, but rather an trace of the overcompressive nature of the limiter. The iterative convergence history of the two schemes are also different. The MUSCL results are converged, while we are not able to drive the iterative residual to machine lower than 10^{-2}–10^{-3}. This seems related to the behavior of the Lax Friedrichs PSI scheme of Section 2.5.

The RD schemes seems much less dependant on the quality of the mesh. This point is illustrated in Fig. 11. This is the NACA012 case, the Mach number is $M = 0.85$ and the angle of attack is $\alpha = 1°$. The mesh is displayed in Fig. 10, and is of poor quality, in purpose. The MUSCL results exhibit a very strong numerical boundary layer that does not appear in the RD results. The boundary conditions are identical, so this is an indication of the numerical dissipation of the scheme. Indeed, the boundary conditions at the nose of the airfoil generates entropy. The MUSCL scheme convect and increases this, while the RD scheme has a much lower influence.

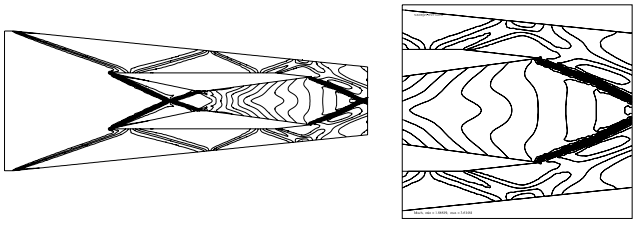

Fig. 7. Isolines of the Mach number, scramjet problem, MUSCL scheme. Min = 1.868, Mach = 3.61.

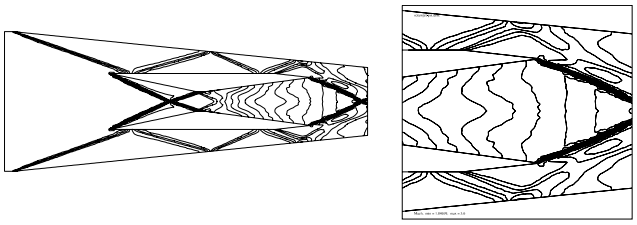

Fig. 8. Isolines of the Mach number, scramjet problem, PSI scheme, Min = 1.847, Mach = 3.6.

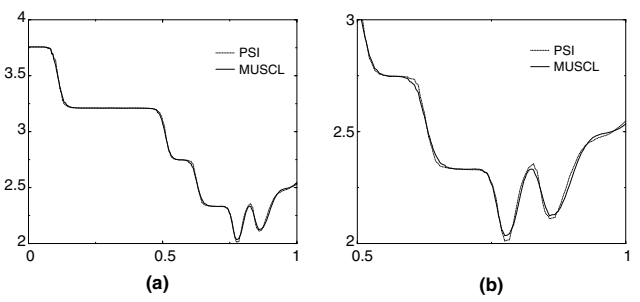

Fig. 9. Cross-section of the mach number (a) and zoom (b) along a parallel in the bottom channel.

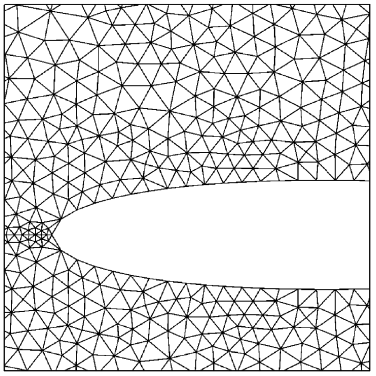

Fig. 10. Mesh for the NACA012 test case.

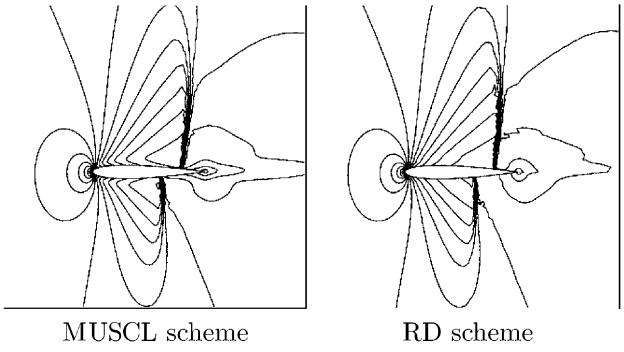

Fig. 11. Solutions for the NACA012 test case.

2.9. Formulation, FE view point, formulation for viscous problems

In this section, we provide some bridges between stabilised finite elements methods such as the SUPG method of Hughes, and the high order residual schemes above. Indeed we provide several interpretations in the scalar case that can be easily extended to the system case, and show that some of these formulations can simplify, and clarify, the extension to these schemes to convection diffusion problems.

2.9.1. Finite element formulations

It is interesting to look at (10) from a more abstract point of view in order to connect the RD schemes to more known schemes. In the previous sections, the idea was to increase the formal order of accuracy starting from a first order scheme in such a way that oscillations are controlled. This was done by borrowing ideas from the high order nonoscillatory schemes such as the TVD scheme because the main trick is to compare the total residual to the first order residuals.

In what follows, we connect them to the SUPG schemes and more generally to finite element type schemes. To make things simple, we consider the advection problem $\mathbf{a}\cdot\nabla u = 0$ on Ω with Dirichlet boundary conditions on the inflow part of $\partial\Omega$. We start from (10). If φ is any compactly supported continuously differentiable function, we have equivalently

$$\sum_{M_i}\varphi_i\left(\sum_{T\ni M_i}\Phi_i^{\mathrm{T}}\right)=0,$$

that is

$$\sum_{T\subset\Omega}\sum_{M_j\in T}\varphi_j\Phi_j^{\mathrm{T}}=0.$$

Then we introduce $\bar\varphi_T=\frac{\varphi_{i_1}+\varphi_{i_2}+\varphi_{i_3}}{3}$ the value of the continuous piecewise linear interpolant φ^h of the nodal values $\{\varphi_j\}_{j=1,\dots,n_s}$. Using the conservation relation (11), we get

$$\sum_{T\subset\Omega}\bar\varphi_T\int_T\mathbf{a}\cdot\nabla u^h\,\mathrm{d}x+\sum_{T\subset\Omega}\left(\sum_{M_j\in T}(\varphi_j-\bar\varphi_T)\Phi_j^{\mathrm{T}}\right)=0.$$

Now, because $\mathbf{a}\cdot\nabla u^h$ is constant over any triangle T, and because of the exactness of the quadrature formula for linear functions,

$$\int_T\varphi^h\,\mathrm{d}x=|T|\bar\varphi,$$

this equation can be rewritten as

$$\int_\Omega\varphi^h\mathbf{a}\cdot\nabla u^h\,\mathrm{d}x+\sum_{T\subset\Omega}\left(\sum_{j\in T}(\varphi_j-\bar\varphi_T)\Phi_i^{\mathrm{T}}\right)=0.$$

The last step is to consider now a LP scheme for which $\Phi_i^{\mathrm{T}}=\beta_i^{\mathrm{T}}\Phi^{\mathrm{T}}$, we see that

$$\sum_{j\in T}(\varphi_j-\bar\varphi_T)\Phi_i^{\mathrm{T}}=\sum\nolimits_{j\in T}(\varphi_j-\bar\varphi_T)\beta_j^{\mathrm{T}}\int_T\mathbf{a}\cdot\nabla u^h\,\mathrm{d}x$$
$$=h\int_T(\vec\xi_T\cdot\nabla\varphi^h)(\mathbf{a}\cdot\nabla u^h)\,\mathrm{d}x,$$

where

$$h\vec\xi_T\cdot\nabla\varphi^h=\sum_{j\in T}(\varphi_j-\bar\varphi_T)\beta_j^{\mathrm{T}}=\left(\sum_{j\in T}\beta_j^{\mathrm{T}}\vec{M_jG}\right)\cdot\nabla\varphi^h,\quad(30)$$

i.e. $h\vec\xi_T:=\sum_{j\in T}\beta_j^{\mathrm{T}}\vec{M_jG}$. Thus, the scheme results into

$$\int_\Omega\varphi^h\mathbf{a}\cdot\nabla u^h\,\mathrm{d}x+h\int_\Omega(\vec\xi\cdot\nabla\varphi^h)(\mathbf{a}\cdot\nabla u^h)\,\mathrm{d}x=0\quad(31)$$

with $\vec\xi_{|T}=\vec\xi_T$. We notice that $\vec\xi$ is uniformly bounded.

The relation (31) suggests a way to implement the Dirichlet boundary conditions $u=g$ on Γ^-,[2] namely

$$\int_\Omega v^h\mathbf{a}\cdot\nabla u^h\,\mathrm{d}x+\sum_{T\subset\Omega}h\int_T(\vec\xi\cdot\nabla v^h)(\mathbf{a}\cdot\nabla u^h)\,\mathrm{d}x$$
$$-\int_{\Gamma^-}gv^h\,\mathrm{d}l=0\quad(32)$$

and v^h, u^h belongs to the set of continuous piecewise linear functions V^h.

The relation (32) can be abstractly reformulated as: find $u^h\in V^h$ such that for all $v^h\in V^h$,

$$a(u^h,v^h)=l(v^h),$$

with

$$l(v^h)=\int_{\Gamma^-}gv^h\,\mathrm{d}l$$

and

$$a(u,v)=\int_\Omega v\mathbf{a}\cdot\nabla u\,\mathrm{d}x+h\int_\Omega(\vec\xi\cdot\nabla v)(\mathbf{a}\cdot\nabla u)\,\mathrm{d}x$$
$$\equiv\int_\Omega\omega^h\mathbf{a}\cdot\nabla u\,\mathrm{d}x,$$

where ω^h is *discontinuous* across edges.

It is interesting to notice that this formulation is not unique. In fact, we have followed the inverse path as usually done. In general, given a PDE, a finite element space is considered on which a consistent formulation, compatible with the definition of the finite element space and the PDE, is given. Here we have stated from an algebraic relation, namely (10) and we have reinterpretated it in a finite element flavour, with some a priori choices. Here this leads to (30) and (31) which looks as the SUPG formulation.

Other numerically equivalent formulations can be obtained. For any triangle T, the problem is to find a set

[2] However, in all the numerical tests of the paper, the Dirichlet boundary conditions have been enforced strongly.

of three linearly independent functions Ψ_i^T for which we have

$$\beta_i^T \int_T \mathbf{a}\cdot\nabla u^h \,dx = \int_T \Psi_i^T \mathbf{a}\cdot\nabla u^h \,dx.$$

Once more we use the fact that u^h being linear, $\mathbf{a}\cdot\nabla u^h$ is constant, so the constraint is

$$\beta_i^T |T| = \int_T \Psi_i^T \,dx.$$

A solution to this problem is $\Psi_i^T = (\mathcal{N}_i)_T + \gamma_i^T b^T$ where b^T is any continuous function such that $\int_T b^T dx > 0$ and b^T vanishes on the boundary of T. An example is given and described in Fig. 12. The coefficient γ_i is then defined by

$$\gamma_i^T = \frac{\beta_i^T - \frac{1}{3}}{\int_T b^T dx}.$$

We note that the example of Fig. 12 satisfies $\int_T \nabla b^T dx = 0$.

Once γ_i^T is defined, we define the test function Ψ_i by $(\Psi_i)_{|T} = \Psi_i^T$ and the set of test functions W^h as the span of $\{\Psi_i\}_{i=1,\dots,n_s}$. If once more V_h is the set of continuous piecewise linear functions, and avoiding the important problem of the boundary conditions, we have a Petrov–Galerkin variational formulation of the scheme: find $u^h \in V^h$ such that for all $w^h \in W^h$,

$$\int_\Omega w^h \mathbf{a}\cdot\nabla u^h \,dx = l(w^h). \tag{33}$$

The main difference between this formulation and the SUPG like is that the test functions are now *continuous* across the edges of the triangulation. The two constructions, SUPG like or with bubble like test functions, can be generalised to the system problem without major difficulty.

2.9.2. Application to viscous problems

Once more we focus on the scalar problem

$$\begin{aligned} &\mathbf{a}\cdot\nabla u - \nabla\cdot(K\nabla u) = 0 \quad x\in\Omega,\\ &u = g \quad x\in\partial\Omega, \end{aligned} \tag{34}$$

where K is a symmetric positive definite constant matrix for simplicity. We use a variational formulation with the same test functions as in the previous paragraph. Formally, we would have to find u^h in V^h (space of continuous piecewise linear test functions) such that for any test function in W^h,

$$\int_\Omega w^h \mathbf{a}\cdot\nabla u^h \,dx - \int_\Omega w^h \nabla\cdot(K\nabla u)\,dx = 0.$$

Of course the term $\int w^h \nabla\cdot(K\nabla u)\,dx$ has no meaning, so we integrate by part thanks to the divergence theorem,

$$\begin{aligned} \int_\Omega w^h \nabla\cdot(K\nabla u)\,dx &\equiv \sum_T \int_T w^h \nabla\cdot(K\nabla u)\,dx\\ &= \sum_T \left(\int_{\partial T} w^h (K\nabla u)\cdot\vec{n}\,d\sigma - \int_T \nabla w^h\cdot(K\nabla u^h)\,dx \right). \end{aligned}$$

If w^h is continuous, then the first term of the last line of (2.9.2) vanishes because this sum can be rewritten as a sum on edges, where each term appears twice, once with a $+\vec{n}$, once with a $-\vec{n}$. This property is not true when w^h is not continuous. For this reason, we prefers the formulation (33) where the test functions are continuous by construction. A closer look at $\int_T \nabla w^h\cdot(K\nabla u^h)\,dx$ reveals some additional simplifications.

$$\begin{aligned} \int_T \nabla\Psi_i^T\cdot(K\nabla u^h)\,dx &= \int_T \nabla\mathcal{N}_i\cdot(K\nabla u^h)\,dx\\ &\quad + \gamma_i^T \int_T \nabla b^T\cdot(K\nabla u^h)\,dx. \end{aligned}$$

Then, $K\nabla u^h$ is a constant, and since $\int_T \nabla b^T = 0$, the second term vanishes.

In summary, the formulation is to find u^h such that for any vertices,

$$\sum_{T\ni M_i} \Phi_i^T + \sum_T \int_T \nabla\mathcal{N}_i\cdot(K\nabla u^h)\,dx = 0.$$

In other words, the convective terms are discretised with the LP residual distribution scheme and the dissipative terms are discretised with a classical Galerkin approximation.

This fact has been used in many papers, but the method was presented uncorrectly from a mathematical point of view. The SUPG-like Petrov Galerkin approximation was used and the viscous terms were approximated by a Galerkin formulation, so *neglecting* all the annoying terms. The numerical results were good, and even surprisingly good in term of accuracy: the scheme should have been first order only, and it was not. Our analysis shows that the "neglected" terms does not appear indeed, and more over, the scheme satisfies the variational formulation (2.9.2) where the test functions have a square integrable gradient. Then it becomes standard to show that the expected order of accuracy is indeed met, provided the stability of the scheme is shown. We do not know how to show the stability of the scheme (except in the maximum norm which is not suitable for this analysis), so the analysis is not complete, but it is a strong indication of the correctness of our approach.

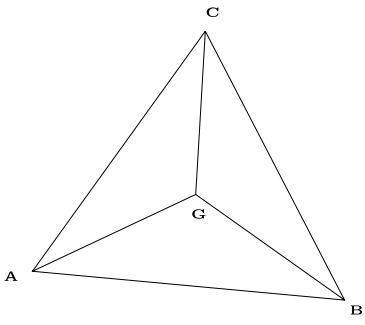

Fig. 12. An example of a bubble function. b_T vanishes on the boundary of T and is linear in each of the sub-triangles (ABG), (BCG), (CGA).

3. RD for unsteady problems

This part summarise [18]. An other possible construction is described in [40].

3.1. Construction

For simplicity, we consider the problem (1) with a constant advection speed. Let T be any triangle, we denote by K the time–space prism $K = T\times[t_n, t_{n+1}]$, see Fig. 13. The numerical solution of (1) is interpolated in K linearly in time and space, namely

$$u^h(x,t) = u^{n+1}(x)\frac{(t-t_n)}{\Delta t} + u^n(x)\frac{(t_{n+1}-t)}{\Delta t}, \tag{35}$$

where u^n (respectively u^{n+1}) is the linear interpolation of $\{u^n_{j_1}, u^n_{j_2}, u^n_{j_3}\}$ (respectively $\{u^{n+1}_{j_1}, u^{n+1}_{j_2}, u^{n+1}_{j_3}\}$). Then, we consider the total residual in K,

$$\Phi^K := \int_{t_n}^{t_{n+1}}\int_T \left(\frac{\partial u}{\partial t} + \mathbf{a}\cdot\nabla u\right)\mathrm{d}x\,\mathrm{d}t.$$

If $\vec{n}_i$ is the inward scaled normal opposite to M_i in T, setting $k_i = \frac{1}{2}\mathbf{a}\cdot\vec{n}_i$, we have

$$\Phi^K = \frac{|T|}{3}\sum_{j=1}^{3}(u_j^{n+1}-u_j^n) + \frac{\Delta t}{2}\sum_{j=1}^{3}k_i(u_j^{n+1}+u_j^n).$$

The idea is to split Φ^K into sub-residual that the prims K "sends" to its six vertices, and then for any vertex to gather the sub-residuals in order to update the solution. Then, the definition of the sub-residuals Φ_i^K uses the causality principle: the past does not depend on the future. This means that the sub-residuals sent by K to the vertices $(M_j, t_n)_{j=1,3}$ are set to zero, i.e., only the residual sent to $(M_j, t_{n+1})_{j=1,3}$ may be nonzero. They are denoted by Φ_j^K. This enables to decouple the time slabs. Then, conservation is garantied provided the following relation holds

$$\sum_{M_j\in T}\Phi_j^{\mathrm{T}} = \Phi^K. \tag{36}$$

Last, the scheme is defined by

$$\sum_{T\ni M_i}\Phi_i^K = 0. \tag{37}$$

This represents a system of equations of the form $F(U^{n+1}, U^n) = 0$ where U^n (respectively U^{n+1}) represents the vector of unknown variables at time t_n (respectively t_{n+1}). Since U^n is known, this equation is solved in U^{n+1}, and then we can repeat the procedure to iterate in real time.

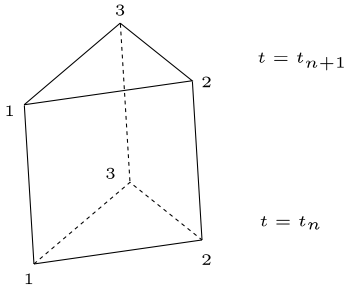

Fig. 13. A representation of $K = T\times[t_n, t_{n+1}]$.

The last thing to do is to precisely define the sub-residuals. One guiding principle is that some stability property holds, for example stability in L^∞, the other one is accuracy.

3.1.1. Stability requirements

An example of such a scheme is provided by the N scheme:

$$\Phi_i^K = \frac{|T|}{3}(u_i^{n+1}-u_i^n) + \frac{\Delta t}{2}(k_i^+(u_i^{n+1}-\tilde{u}^{n+1}) + k_i^+(u_i^n-\tilde{u}^n)),$$
$$\tilde{u}^{n+1,n} = n\left(\sum_{j=1}^{3}k_j^- u_j^{n+1,n}\right), \quad n = \left(\sum_{j=1}^{3}k_j^-\right)^{-1}. \tag{38}$$

The N scheme in (37) leads to an equation of the form $Au^{n+1} = Bu^n$ where A and B are constant matrices. A closer analysis reveals that A is a monotone matrix, whatever Δt, and that B has positive coefficients provided the CFL-like condition holds $\Delta t\max_T\frac{\sum_{j\in T}k_j^+}{|T|}\leqslant 1$. This shows that the N scheme is L^∞ stable under a CFL-like condition. In fact, the analysis is not sharp enough, and numerical experiments demonstrate that this condition may be violated by a large factor. A deaper analysis also shows that the N scheme is *unconditionally* L^2 stable, see [18] for details.

Following Ricchiutto [22], a variant of the N scheme is

$$\Phi_i^{\mathrm{T}} = \frac{|T|}{3}(u_i^{n+1}-u_i^n) + \Delta t k_i^+(u_i^{n+1}-\tilde{u}^{n+1}) \tag{39}$$

together with (37). This leads to a linear system of the form $Au^{n+1} = u^n$ where A is a monotone matrix whatever Δt, so that the scheme is unconditionally L^∞ stable. This is detailed in Appendix A as well as the unconditional L^2 stability of the scheme. This scheme is useful in the sequel, even though it does not satisfy the conservation property (36).

3.1.2. Accuracy requirement

The technique is identical to the one described in Section 2.2, since we see the unsteady problem (6) as the steady version of

$$\frac{\partial u}{\partial\tau} + \left(\frac{\partial u}{\partial t} + \mathbf{a}\cdot\nabla u\right) = 0,$$

hence we can use the same tools.

In [14] for steady problems and in [18] for second order schemes, it is shown that, provided the *exact* solution of (1) is smooth, the scheme is formally second order in time and space provided that for all triangle T and any vertex, we have

$$\Phi_i^K = \mathcal{O}(h^3, \Delta t^2),$$

where h is the maximum radius of the triangles T. The derivation of this condition also need that the mesh be regular in the usual finite element meaning. There are several ways

of fulfilling this condition [4,13,18], the easiest one being the Linear Preserving as in Section 2.5. In the next paragraph, we sketch how to construct schemes that are both LP and L^∞ stable following the same logic as in (2.5). We only point out the differences.

3.1.3. Accuracy and stability

In order to fulfill this goal, we consider a first order monotone scheme which residuals are $\{\Phi_i^L\}$, and we want to construct a second order scheme $\{\Phi_i^H\}$ such that $\Phi_i^H = \beta_i \Phi^K$ with β_i uniformly bounded so that accuracy is guaranteed, and such that this scheme, coupled with (37), still satisfies a maximum principle.

To this end, we use any of the space–time variants of the N scheme (38) or (39) as a low order scheme Φ_i^L. We note that the residual sent at the vertices of T but for the time t_n are identically 0 by construction, so it will be the same for the limited second order scheme. Thus we only have three β coefficient, they correspond to the amount of the total residual

$$\Phi^K = \frac{|T|}{3}\sum_{j=1}^{3}(u_j^{n+1}-u_j^n) + \frac{\Delta t}{2}\sum_{j=1}^{3} k_i(u_j^{n+1}+u_j^n),$$

sent to the vertices of T at time t_{n+1}. A possible formula is given by (25) where once more

$$x_i = \frac{\Phi_i^L}{\Phi_K}.$$

The rest is similar.

Remark 3.1 (*Stability*). The scheme we have sketched here is monotone under a CFL condition, as its scalar version was. This is a bit disappointing since it is a fully implicit scheme. In [17], we show that the N scheme above is unconditionally energy stable, but no such result seems available in the maximum norm, even though in practice the CFL constraint can be violated. Csik has imagined in his PhD thesis a N scheme that is unconditionally stable in the maximum norm, [41]. This version is more complicated than the one presented here because instead of the tetrahedral space–time element for the total residual he uses prismatic space–time elements resulting in a quite complex space–time mesh. This idea has been adapted by Mezine in his thesis [42] to the prismatic space–time element. The method is successful, results can be seen in [17]. Very large CFL number can be used. This method has been further simplified by Ricchiuto, see [21,22].

3.2. Numerical examples

3.2.1. Scalar problems

3.2.1.1. The rotating cosine hill. The rotating cosine hill is a classical test-case for numerical schemes of the two-dimensional linear unsteady advection equation. The test consists in the transport of a cosine shape by a circular solid body advection field centered at the origin

$$\frac{\partial u}{\partial t} + \mathbf{a}\cdot\nabla u = 0 \quad \text{in } [-1,1]\times[-1,1], \tag{40}$$

where $\mathbf{a} = (y,-x)^{\mathrm{T}}$. The initial solution is

$$u_0(x,y) = \begin{cases} \left(1+\cos(4\pi\sqrt{(x+0.5)^2+y^2})/2\right) \\ \quad \text{if } r = \sqrt{(x+0.5)^2+y^2} \leqslant \frac{1}{8}, \\ 0 \quad \text{else.} \end{cases}$$

The solution is set to zero at the inflow boundaries, at each time step.

The computation was made on a unstructured grid of 8079 nodes and 15836 elements. The time step was taken to satisfy the condition:

$$\Delta t = \frac{2}{3}\mathrm{CFL}\min_i \frac{|T|}{k_i^+} \tag{41}$$

with CFL = 0.9. The results, using the schemes described in the previous section and the MUSCL scheme (with *min-mod* limiter and Runge–Kutta integration in time) after one revolution are compared in Fig. 14. We provide the cross-section at $y = 0$ in Fig. 15. The N-scheme is clearly the most diffusive (see also Table 1), streamwise and crosswise diffusion are considerable. The LDA scheme keeps the height of the peak much better but the monotonicity is not preserved. This results are much better than those obtained by the MUSCL scheme.

3.2.1.2. The rotating cylinder. This test case differs from the previous only for the initial profile

$$u_0(x,y) = \begin{cases} 1 & \text{for } r < 0.25, \\ 0 & \text{else,} \end{cases} \tag{42}$$

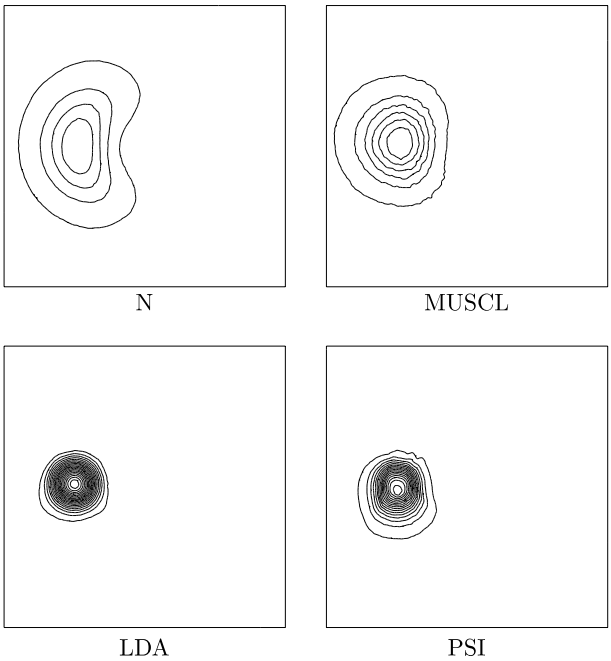

Fig. 14. Solutions for the rotating cosine hill after one revolution.

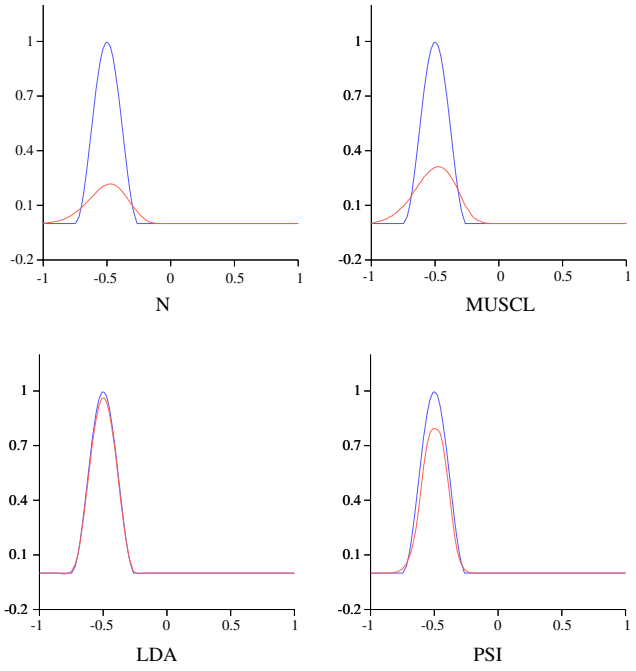

Fig. 15. Sections at $y = 0$ of the solutions for the rotating cosine.

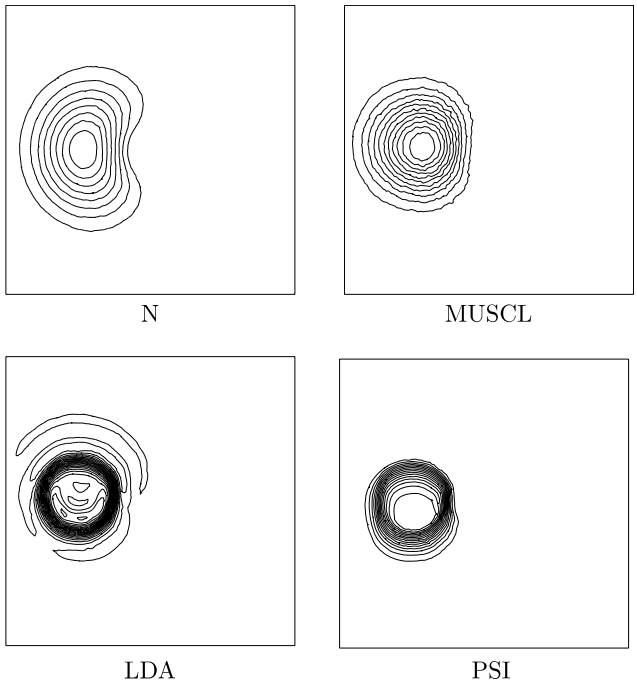

Fig. 16. Solutions for the rotating cylinder after one revolution.

Table 1
Min and Max solution values for the rotating cosine hill test case

Scheme	Min	Max
N	0	0.217
MUSCL	0	0.313
LDA	−0.03	0.983
PSI	0	0.802

where $r = \sqrt{(x+0.5)^2 + y^2}$, which is not continuous, contrary to the previous case. The computation was made on the same grid with a CFL of 0.9, the results after one revolution are displayed in Fig. 16. The solutions exhibit the same properties as the rotating cosine hill. Cross-sections of the solutions after one revolution are provided in Fig. 17. This results are better than MUSCL scheme. The LDA scheme exhibits spurious oscillations, as expected.

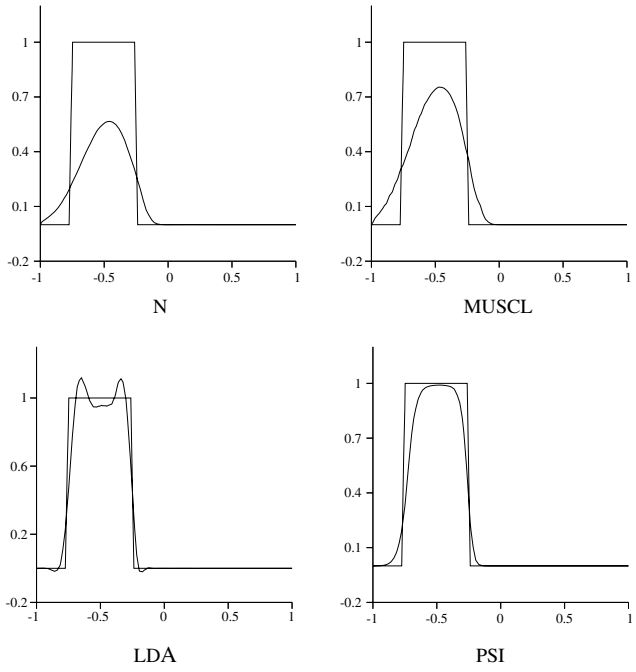

Fig. 17. Sections at $y = 0$ of the solutions for the rotating cylinder.

3.2.2. Flow problems

Before giving some numerical examples, let us explain how we use the results of Section 3.1. In fact, we proceed exactly as in Section 2.6. For each element T, we first chose a direction (in practice the flow direction, but any other would do). Call θ_T the angle so defined, and consider the eigenvectors of $\cos\theta_T A + \sin\theta_T B$ where A and B are the Jacobian matrices in the x- and y-directions evaluated at the average Roe state. As before we denote these right eigenvectors by $\{r_\xi\}_\xi$ and by $\{\ell_\xi\}_\xi$ the set of left eigenvectors. Then, given the space–time residuals Φ_i, $i = 1, \ldots, 3$ and the total residual $\Phi = \Phi_1 + \Phi_2 + \Phi_3$, we project these quantities onto the right eigenvectors and define directional space–time residuals,

$$\varphi_i^\xi = \ell_\xi^{\mathrm{T}} \Phi_i$$

and notice that

$$\sum_j \varphi_i^\xi = \ell_\xi^{\mathrm{T}} \Phi := \varphi^\xi.$$

The rest follows exactly as in Section 2.6. In the rest of this section we present results on some classical test cases.

3.2.2.1. A two-dimensional Riemann problem. The initial data are chosen in order to represent a "2D Sod tube" in the domain $[-1,1]\times[-1,1]$:

$$\begin{cases} \rho = 0.1 & \text{if } x \times y < 0, \quad 1 \quad \text{otherwise} \\ p = 0.1 & \text{if } x \times y < 0, \quad 1 \quad \text{otherwise} \end{cases} \tag{43}$$

and the velocity (u,v) was set to zero. The solution is computed at time $t = 0.2$ on a structured triangulation where $\Delta x = \Delta y = 0.01$ and the CFL condition has been set to 0.9.

The isolines of the density and pressure are shown in Figs. 18 and 19 for the N-scheme and the N-modified scheme.

3.2.2.2. A Mach 3 wind tunnel with a forward facing step. This test case has been extensively studied by Woodward and Collela [43], and is widely present in the literature. The setup of the problem is the following: a right-going Mach 3 uniform flow enters a wind tunnel of 1 unit width and 3 units long. The step is 0.2 units high and is located 0.6 units from the left-hand end of the tunnel. The problem is initialized by a uniform, right going Mach 3 flow. Reflective boundary conditions are applied along the walls of the tunnel, and inflow and outflow boundary conditions are applied at the entrance and the exit of the tunnel. The results at time $t = 4$ with the N-scheme and the N-modified scheme are shown. The simulation was done at CFL = 0.9.

The corner of the step is a singularity. It is well known that if no special treatment is done, an entropy production is observed in the vicinity of the step corner, and it alters the quality of the second reflected shock. This is not physical because we have a strong expansion wave, so no entropy should be created. However, unlike in [43], we do not modify our scheme near the corner, because we are only interested in its stability properties.

An unstructured mesh have been considered, it contains 10 868 nodes and 21 281 triangles, it is refined near the corner. Portion of the mesh is shown in Fig. 20.

The quality of the slip line coming out of the triple point is noticeable, as well as the resolution of the shocks, in particular at the exit section of the tunnel. The maximum shock width is no larger than two cells. Between the first order and the second order results, the quality of the fan (at the corner) has dramatically been improved: the reflected shock is now correctly set, the weak compression shock after the fan appears, and interact with the first reflected shock, see the slip line coming out of the interaction between the reflected shock and the weak compression shock (see Figs. 21–24).

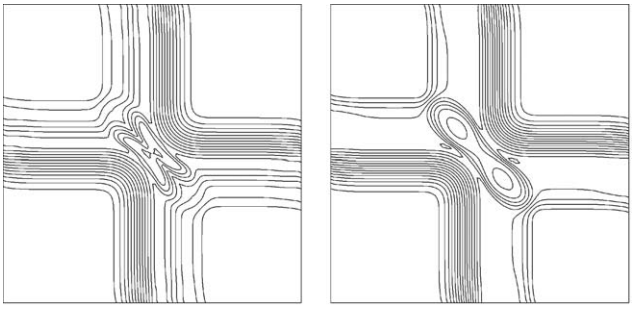

Fig. 18. 2D Riemann problem computed by the N-scheme at time $t = 0.2$, density (left) and pressure (right).

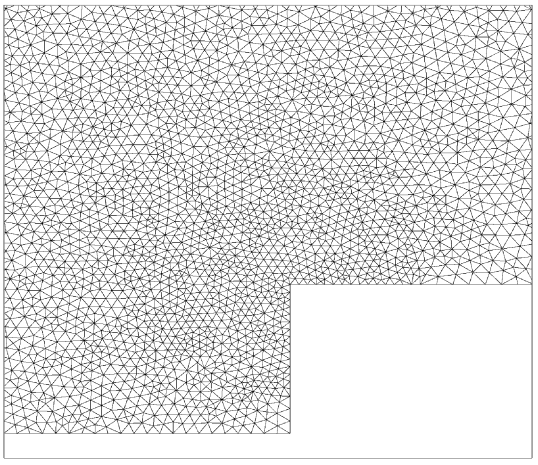

Fig. 20. Part of the unstructured grid for the Mach 3 problem.

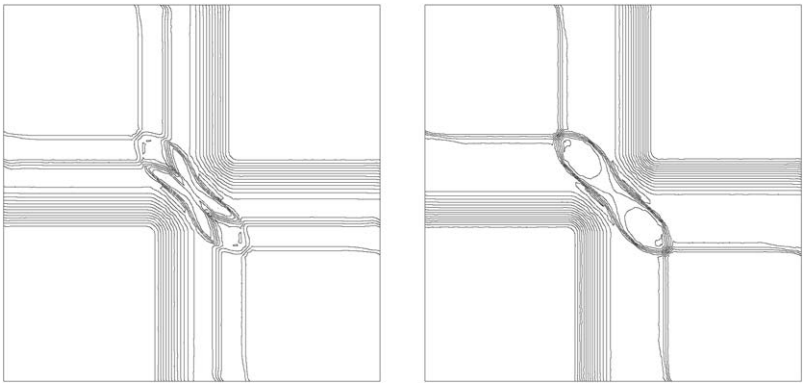

Fig. 19. 2D Riemann problem computed by the N-modified scheme at time $t = 0.2$, density (left) and pressure (right).

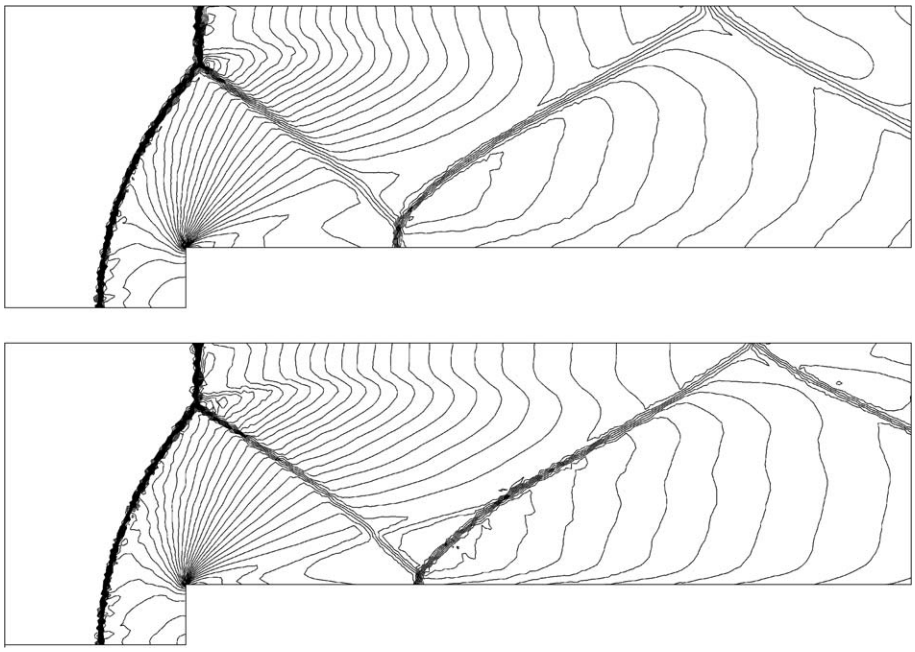

Fig. 21. Forward-facing step problem. Density isolines: 30 equally spaced contour lines from 0.09 to 6.23. Top: N scheme. Bottom: N-modified scheme.

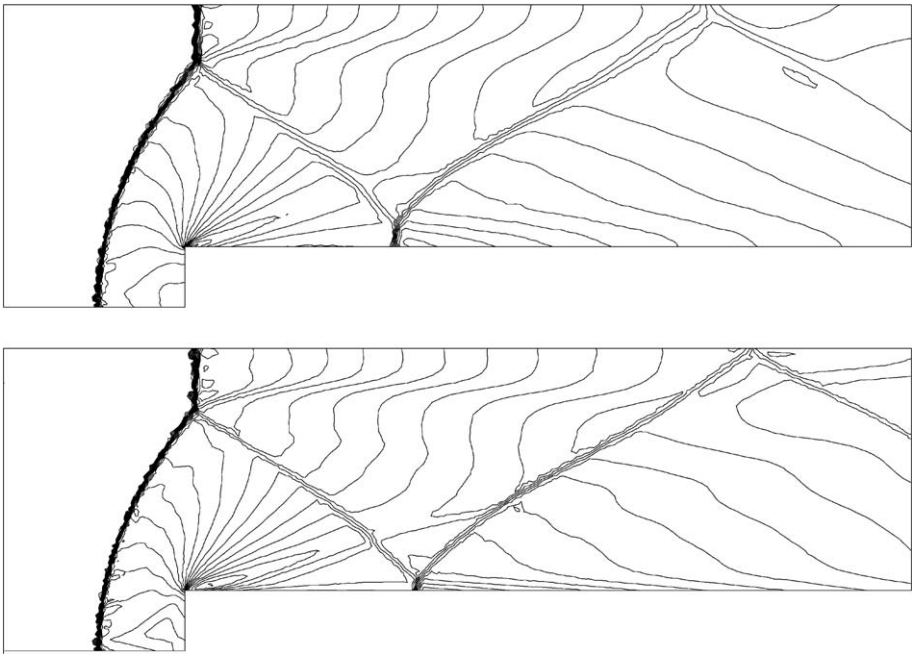

Fig. 22. Forward-facing step problem. Mach number isolines: 25 equally spaced contour lines from 0.02 to 3.82. Top: N scheme. Bottom: N-modified scheme.

3.2.2.3. Reflection of a shock on a wedge. This problem was studied by Quirk [44]. A planar shock initially enters from the left in a quiescent fluid and is reflected from a 45° ramp. Its Mach number is $M_s = 5.5$ and is defined toward the flow values in the quiescent fluid where the density is set to 1.4 and the pressure to 1. Reflective boundary conditions are applied along the ramp and the bottom and the upper of the problem domain. For such an incident shock wave Mach number and such a reflecting wedge angle, a double Mach reflection is expected. The interest of this test case is that, according to [45], the angle $\theta = 45°$ and $M_s = 5.5$ is nearly at the transition between a double Mach reflection

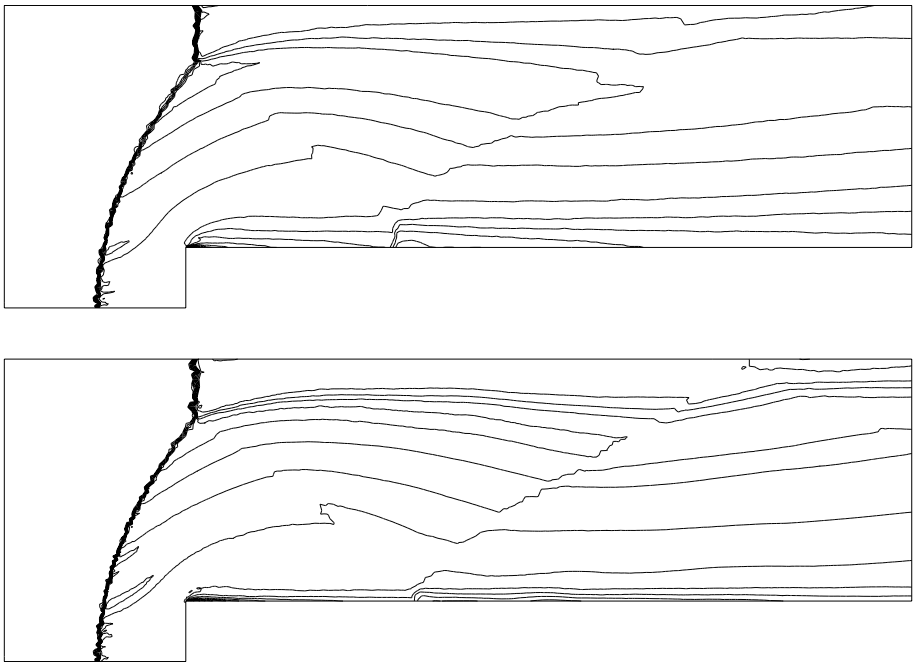

Fig. 23. Forward-facing step problem. Entropy production near the step corner: 17 equally spaced contour lines from 0.63 to 1.5. Top: N scheme. Bottom: N-modified scheme.

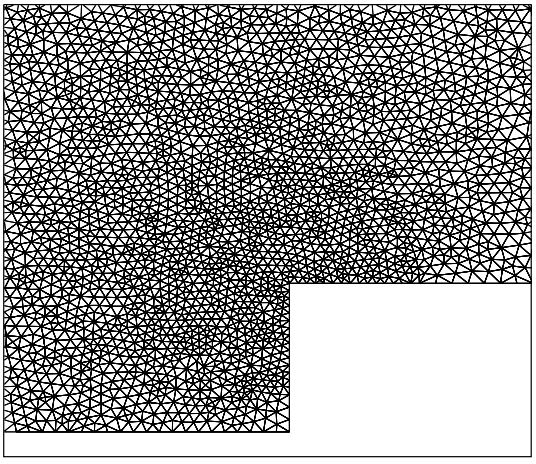

Fig. 24. Part of the unstructured grid.

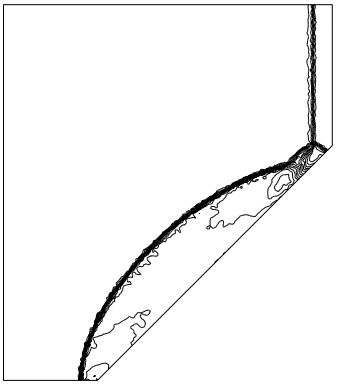

Fig. 25. Reflection of a planar shock from a ramp. Density 20 contour lines from 1.18 to 20.12.

and a regular reflection. If the scheme were too diffusive, we would get a regular reflection instead of a double Mach reflection. Hence this is a good test of accuracy.

The density is displayed in Fig. 25. The resolution of the different structure is quite clean, despites the poor resolution of the mesh.

3.2.2.4. Shock–vortex interaction problem. This test case describes the interaction between a stationary shock and a vortex. It was first presented by Pao and Salas [46], and was studied by Meadows et al. [47] with a TVD scheme and by Jiang and Shu [48]. The computational domain is taken to be $[0,2]\times[0,1]$. A stationary Mach 1.1 shock is set at $x = 0.5$ and normal to the x-axis. Its left state is $(\rho,u,v,p) = (1,\sqrt{\gamma},0,1)$. A small vortex is superposed to the flow left to the shock and centers at $(x_c,y_c) = (0.5,0.25)$. The vortex is described as a perturbation to the velocity (u,v), temperature $T = \frac{p}{\rho}$ and entropy $S = \ln\frac{p}{\rho^\gamma}$ of the mean flow and denote it by tilde values.

$$\tilde{u} = \epsilon\tau e^{\alpha(1-\tau^2)}\sin\theta, \tag{44}$$

$$\tilde{v} = -\epsilon\tau e^{\alpha(1-\tau^2)}\cos\theta, \tag{45}$$

$$\widetilde{T} = -\frac{(\gamma-1)\epsilon^2 e^{2\alpha(1-\tau^2)}}{4\alpha\gamma}, \tag{46}$$

$$\widetilde{S} = 0, \tag{47}$$

where $\tau = \frac{r}{r_c}$ and $r = \sqrt{(x-x_c)^2+(y-y_c)^2}$. Here ϵ indicates the strength of the vortex, α controls the decay rate of the vortex, and r_c is the critical radius for which the

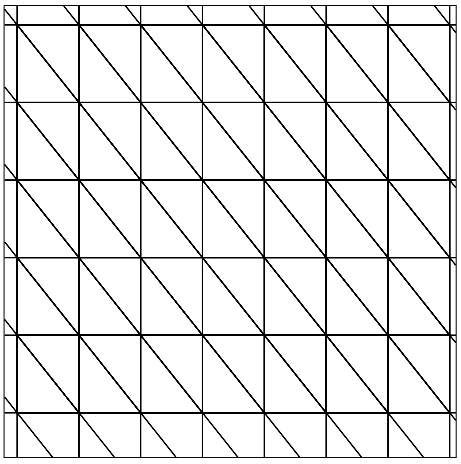

Fig. 26. Zoom of the mesh for the vortex simulation.

vortex has the maximum strength. We choose the same value as in [48], i.e. $\epsilon = 0.3$, $r_c = 0.05$ and $\alpha = 0.204$. The above defined vortex is a steady solution to the 2D Euler equation. The upper and lower boundary are set to be reflective. We use a uniform grid of 251×100, a zoom is shown in Fig. 26. The pressure isolines at three different times are displayed in Fig. 27.

3.2.2.5. Viscous flows. We extend the scheme to viscous flows according to the principles described in Section 2.9. It amounts to "split" the viscous terms and the hyperbolic terms thanks to the correct choice of test functions in the finite element interpretation of the RD schemes. Then a linear interpolation is done in time resulting into a Crank–Nicholson type of approximation. More details can be found in [49]. Taken from this reference, we show and

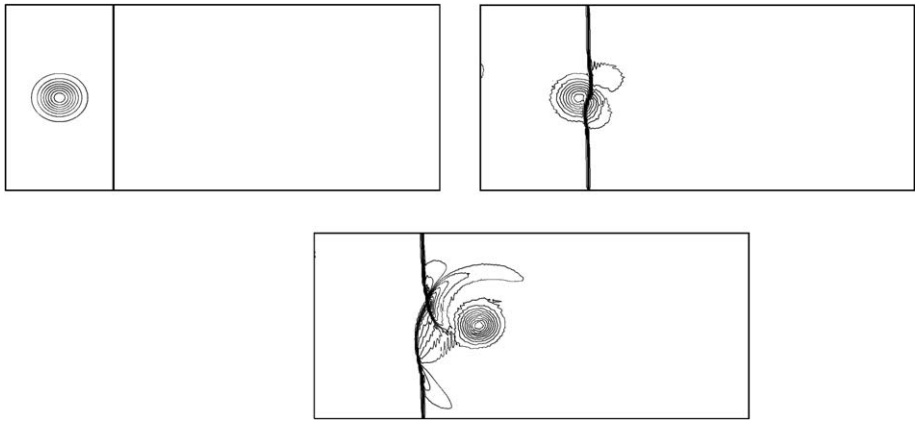

Fig. 27. Shock vortex interaction. Pressure. N-modified scheme. 30 contours lines from 0.84 to 1.4. Top left: $t = 0$; Top right: $t = 0.2$, Bottom: $t = 0.4$.

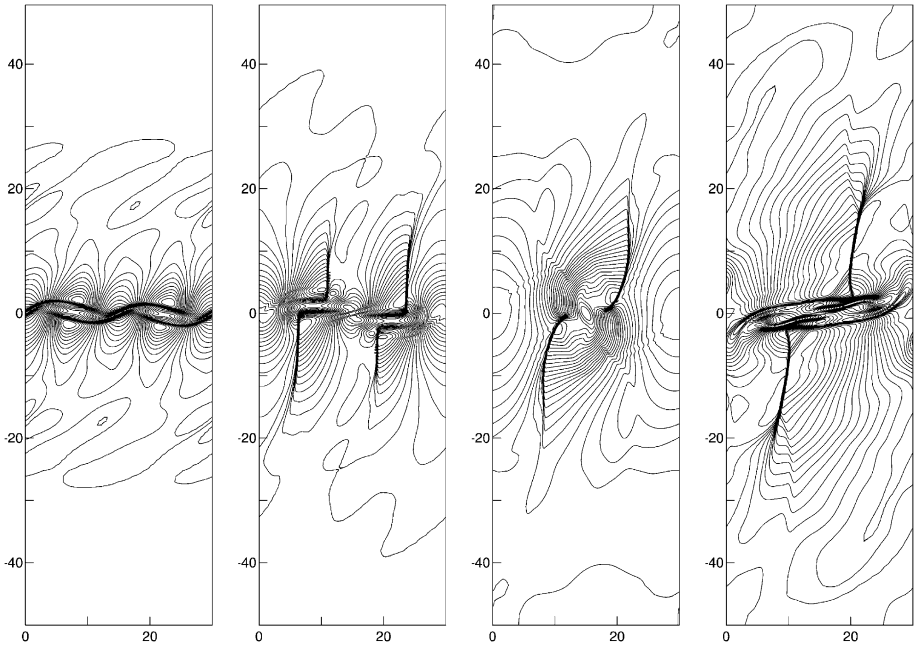

Fig. 28. Isolines of normalized temperature. Figures for $t = 40$, 80, 120, 160, from [49] with permission.

example of a transonic vortex pairing in a mixing layer. This is a well documented test case, see for example [50]. The computation is done in a rectangular box $L_x \times L_y$ with $L_x = 30$ and $L_y = 100$. The Reynolds number is $Re = 1000$ (corresponding to a kinematic viscosity $v_\infty = 10^{-3}$). The Mach number is $M = 0.8$ to which is superimposed a perturbation periodic in the x-direction, and with an exponential decay in the y-direction. The inviscid terms are approximated with the B scheme that corresponds to a blending between the N scheme and the LDA scheme. The blending vector is computed from the residuals. Roughly speaking, the N scheme does no play any role in the smooth part of the flow, where the LDA scheme is dominant tanks to the blending, while the situation is the opposite in discontinuous parts of the flows, see [49,40] for more details. Note that in the scalar case, a special choice of the blending parameter leads to the scalar PSI scheme, see [14] for details.

The solutions at times $t = 40$, 80, 120, 160 are shown in Fig. 28, where 30 levels of isolines of the temperature are plotted. Comparing with the fourth order results of [50], the method shows all features of flow-field which is very satisfactory for a method that is only second order accurate, at most.

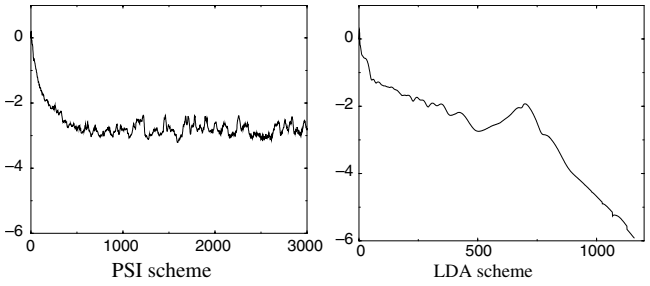

Fig. 29. Convergence history for the PSI scheme of Section 2.5 and the LDA scheme. We have represented $\log_{10}$ of the L^2 norm of the density component of $\sum_{T \ni M_i} \Phi_i^T$.

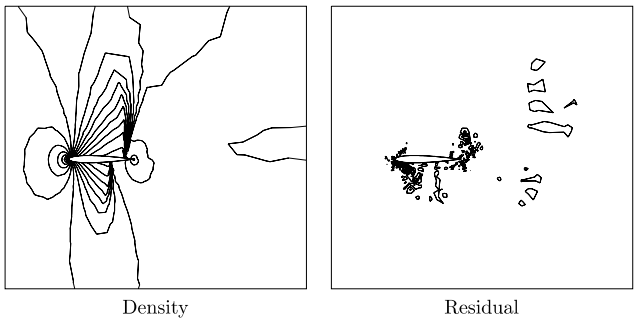

Fig. 30. Density field and isolines of the density residual for the NACA 012 case, and the PSI scheme.

4. Problems and perspectives

4.1. Problems for second order schemes

As pointed out several time in the text, the RD methods end up by solving a nonlinear equation of the type

$$\Psi(U, U_{\text{boundary}}) = 0$$

in the steady case and

$$\Psi(U^{n+1}, U^n, U_{\text{boundary}}) = 0$$

in the unsteady one. The operator Ψ (i.e. the scheme itself) is written in such a way that no explicit solution is possible in the second order limited case. A closer examination of the equation reveals that for the first order case, the problem amounts to solve a large linear system, and the same is true for second order LP scheme that are nonlimited as for the LDA scheme. It is of fundamental importance that these equations are solved correctly and efficiently. By correctly, we mean that the left-hand side, 0 here, may be replaced by a small term of the order of the truncation error, otherwise accuracy is lost.

In practice, these equations are solved by an iterative method, using a preconditioning technique. For steady problems, first, we precondition the second order scheme (limited or unlimited) by a first order scheme. Very often in the limited case, the convergence behavior of the iterative method, after a very nice startup, becomes chaotic. A typical example is given in Fig. 29. It represents the convergence history for the PSI scheme of Section 2.5 for the NACA 012 test case, $M_\infty = 0.85$ one degree of incidence and CFL = 50. The implicit phase is solved with GMRES with ILU preconditioning. In Fig. 30, we provide the isolines of the density, as well as those of the density component of $Res = \sum_{T \ni M_i} \Phi_i^T$. There is no apparent correlation between the high values of Res_ρ and the structure of the density field. In particular, one would expect that the high values correspond to the shocked regions of the flow-field, this is not the case.

This chaotic behavior does not exist for the LDA scheme, see Fig. 29, or the blended scheme in its versions of [24] or [14] as sketched in Section 2.7, once (29) has been suitably implemented.

Concerning unsteady problems, we observe similar chaotic convergence behavior in the solution of the pseudo-time marching part of the algorithm.

Fortunately, this behavior does not seem to affect the quality of the solutions, as demonstrated in the previous section, but this is not satisfactory. We note that for unsteady simulations, 4–5 implicit iterations are enough to reach a low enough residual as experiments indicate. The fundamental reasons of such a behavior are not well understood for now, see however [39] for some remedies.

4.2. High order schemes

Until now, we have only considered the case of first and second order accurate schemes. It is possible to construct schemes that are higher than second order accurate for steady and unsteady problems. The case of scalar steady problems is considered in [35,20], that of scalar unsteady

problems in [51]. The case of system problems has not yet been considered.

Let us provide some information about the scalar steady problem, say

$$\begin{aligned} &\mathbf{a}\cdot\nabla u = 0, \quad x\in\Omega,\\ &u = g, \quad x\in\Gamma^- \end{aligned} \tag{48}$$

and consider the case of third order accuracy to fix the ideas. The computational domain is triangulated by a family of triangles. Third order accuracy can be reached in principle for quadratic interpolation. A quadratic polynomial is fully described on each triangle T with six degrees of freedom. Here, we define the degrees of freedom as the values at the vertices of T and the values at the mid-points of the edges of T, see Fig. 31. We denote by σ any of the degrees of freedom in the mesh. In [35], it is shown that if, for any triangle T, one can define residuals $\{\Phi_\sigma^{\mathrm{T}}\}_{\sigma=1,\dots,6}$ such that the following local conservation relation holds

$$\sum_{\sigma\in T}\Phi_\sigma^{\mathrm{T}} = \int_T \mathbf{a}\cdot\nabla u^h\,\mathrm{d}x := \Phi^{\mathrm{T}}, \tag{49}$$

where u^h is the quadratic interpolant of the data, then, as in Section 2.1, the limit solution, if it exists and if it satisfies bounds as in the standard Lax Wendroff theorem, is a weak solution of (48). This result can be extended to the nonlinear case, of course.

In [35], it is also shown that the scheme is third order accurate if the residuals satisfy

$$\Phi_\sigma^{\mathrm{T}} = \mathcal{O}(h^{2+1}). \tag{50}$$

In the d-dimensional case, for a $r+1$th accurate scheme, the condition (50) is replaced by

$$\Phi_\sigma^{\mathrm{T}} = \mathcal{O}(h^{d+r}). \tag{51}$$

The easiest way of fulfilling conditions (50) (or (51) for $r+1$th order of accuracy) is that $\Phi_\sigma^{\mathrm{T}} = \beta_\sigma^{\mathrm{T}}\Phi^{\mathrm{T}}$ where the βs are uniformly bounded.

To construct a high order scheme, the first idea is to construct a first order scheme Φ_σ^L and, as in the previous sections, to upgrade the order of accuracy by defining $\beta_\sigma^{\mathrm{T}}$ by

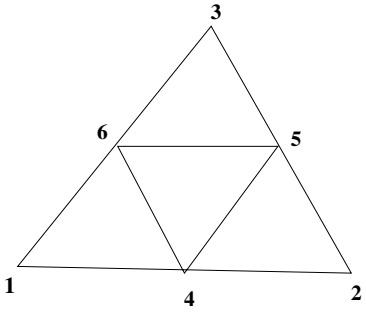

Fig. 31. The six degrees of freedom for quadratic interpolation.

$$\beta_\sigma^{\mathrm{T}} = \frac{\left(\frac{\Phi_i^L}{\Phi^{\mathrm{T}}}\right)^+}{\sum_{j=1}^6\left(\frac{\Phi_j^L}{\Phi^{\mathrm{T}}}\right)^+}. \tag{52}$$

The results (not presented here) are very disappointing, in fact wiggles similar but more pronounced than what is visible in Fig. 5 for the Lax Friedrichs–PSI scheme.

A possible explanation may be the following. In order to define a quadratic polynomials, we need six coefficients. The information contained in (49) is on $\mathbf{a}\cdot\nabla u$, so we loose two degrees of freedom (one for the derivative, one for the dot product), so we have only four degrees of freedom left. The relation (52) define residuals that are all proportional to Φ^{T}, so we do not have enough constraints, and spurious modes may exist.

In [35], we overcome this by the following strategy. From Fig. 31, we can define four sub-triangles defined by $T_\xi = (1,4,6)$, $(4,2,5)$, $(5,3,6)$, $(6,5,4)$. In these four sub-triangles, we can consider the residuals

$$\Phi^{T_\xi} = \int_{T_\xi}\mathbf{a}\cdot\nabla u^h\,\mathrm{d}x.$$

Then, in T_ξ, we consider the N scheme $\Phi_\sigma^{N,\xi}$, and define β_σ^ξ by

$$\beta_\sigma^\xi = \frac{\left(\frac{\Phi_\sigma^{N,\xi}}{\Phi^{T_\xi}}\right)^+}{\sum_{\sigma'\in T_\xi}\left(\frac{\Phi_{\sigma'}^{N,\xi}}{\Phi^{T_\xi}}\right)^+} \tag{53}$$

then

$$\Phi_\sigma^{T_\xi} = \beta_\sigma^\xi\Phi^{T_\xi} \tag{54}$$

and last, the residual sent by T to σ is defined by

$$\Phi_\sigma = \sum_{T_\xi\ni\sigma}\Phi_\sigma^{T_\xi}. \tag{55}$$

Doing so, the total residual in T is splitted in four sub-residuals, and we have enough constraints. This technique can be extended to the nonlinear case, and to fourth order accuracy as well following the same technique, see [35]. We take some results from the same reference.

The main problem of these schemes is that $\sum_{\sigma'\in T_\xi}\left(\frac{\Phi_{\sigma'}^{N,\xi}}{\Phi^{T_\xi}}\right)^+$ in (53) may be zero because

$$\sum_{\sigma\in T_\xi}\Phi^{N,\xi} \neq \Phi^{T_\xi},$$

in general, contrarily to the second order case. This has been noticed by Ricchiuto (VKI). In practice, we replace formula (53) by

$$\beta_\sigma^\xi = \frac{\left(\frac{\Phi_\sigma^{N,\xi}}{\Phi^{T_\xi}}\right)^+ + \varepsilon}{\sum_{\sigma'\in T_\xi}\left(\frac{\Phi_{\sigma'}^{N,\xi}}{\Phi^{T_\xi}}\right)^+ + 3\varepsilon}, \tag{56}$$

where ε is a very small number. When $\sum_{\sigma\in T_\xi}\Phi^{N,\xi}\neq\Phi^{T_\xi}=0$, $\beta_\sigma^\xi=\frac{1}{3}$, so that the scheme is centered, hence unstable on such sub-triangles. We have never experience unstability problems, but we are aware of this unsolved problem.

4.2.1. Linear advection

We consider the problem

$$-y\frac{\partial u}{\partial x}+x\frac{\partial u}{\partial y}=0,\quad (x,y)\in[-1,1]\times[0,1],$$
$$u(x,0)=\begin{cases}0 & \text{if } x\notin[0.1,0.7],\\ \sin\left(\pi\frac{x-0.1}{0.6}\right) & x\in[0.1,0.7].\end{cases}\tag{57}$$

The exact solution is, with $r=\sqrt{x^2+y^2}$, $u(x,y)=\sin(\pi\frac{r-0.1}{0.6})$ if $r\in[0.1,0.7]$ and 0 elsewhere. The numerical solution is computed with a pseudo-time marching algorithm where the initial solution is $u_0=2$.

On each sub-triangle T'_T, we employ the scalar N scheme. The average velocity is defined by

$$(-\bar{y},\bar{x})=\int_T(-y,x)\,\mathrm{d}x\,\mathrm{d}y.$$

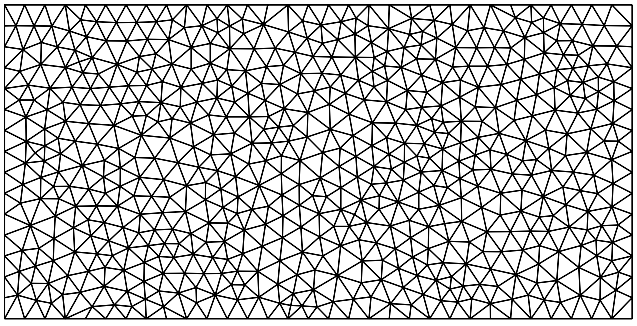

Fig. 32. Mesh for the linear circular advection problem.

Three schemes are compared: the standard second order PSI scheme, a third order scheme and a fourth order one. The high order schemes are constructed using P_3 and P_4 interpolation with the scheme (53)–(55). The mesh has 628 vertices and 1162 elements and is displayed in Fig. 32.

The isolines of the solutions are displayed in Fig. 33. The circular shape of the solution is perfectly well respected in each case. What is more interesting is a plot in the exit section, i.e. for $x=0$ and $y\leqslant-1$. This is given in Fig. 34 with a comparison with the exact one. We also provide a zoom of the solution around $(x,y)=(0,-0.5)$ where the solution is maximum. This figure shows clearly that an increase of the formal accuracy of the scheme does improve its effective accuracy. The fourth order scheme is almost perfect.

Last we provide errors for the advection problem $\mathbf{a}=(0,1)^T$ and the boundary condition $u(x,y)=\cos\pi x$ on $[-1,1]\times[0,1]$. On Fig. 35, we provide the L^2 errors for the second order PSI scheme (Fig. 35a), the third order one (Fig. 35b) and the fourth order one (Fig. 35c). We see that the error slope of the $r+1$ th order scheme is between $r+1/2$ and $r+1$. This is not in contradiction with the expected theoretical $r+1/2$ order of accuracy. In Fig. 36, we display the L^∞ errors: the second order PSI scheme (Fig. 36a), the third order one (Fig. 36b) and the fourth order one (Fig. 36c). We see that the L^∞ errors are closer from the slope $r+1/2$, which seems to indicate that there is no clipping phenomena as in "standard" schemes. However, the fourth order schemes does not provide the expected accuracy, see Fig. 36c. This may be a implementation error, or some roundoff problem (the computations have been performed on a 1 GHz Pentium IV processor with the Intel Fortran 90 compiler, and we have already experienced similar problems on this processor).

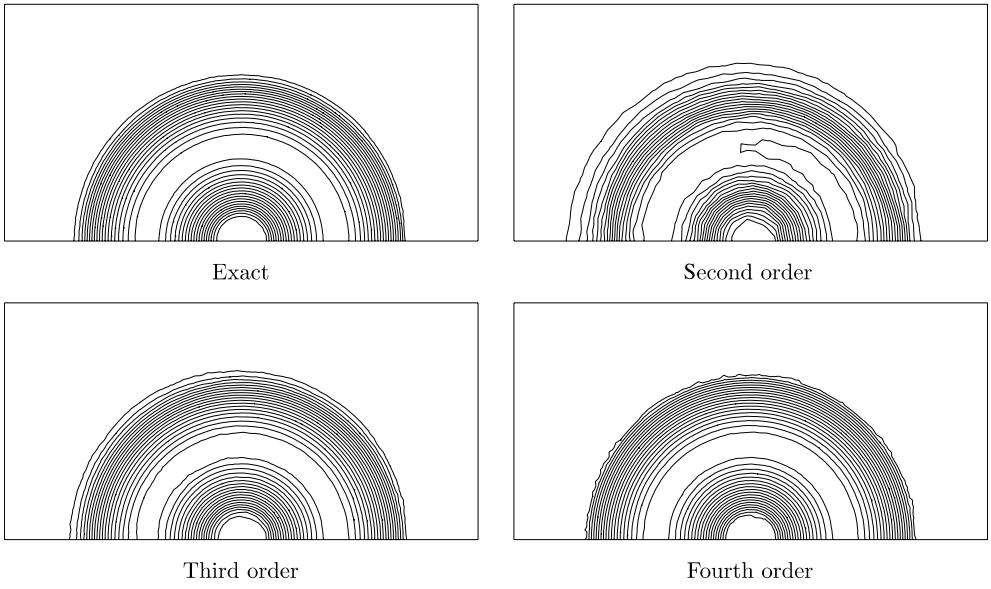

Fig. 33. Isolines of the exact and computed solutions, rotation test.

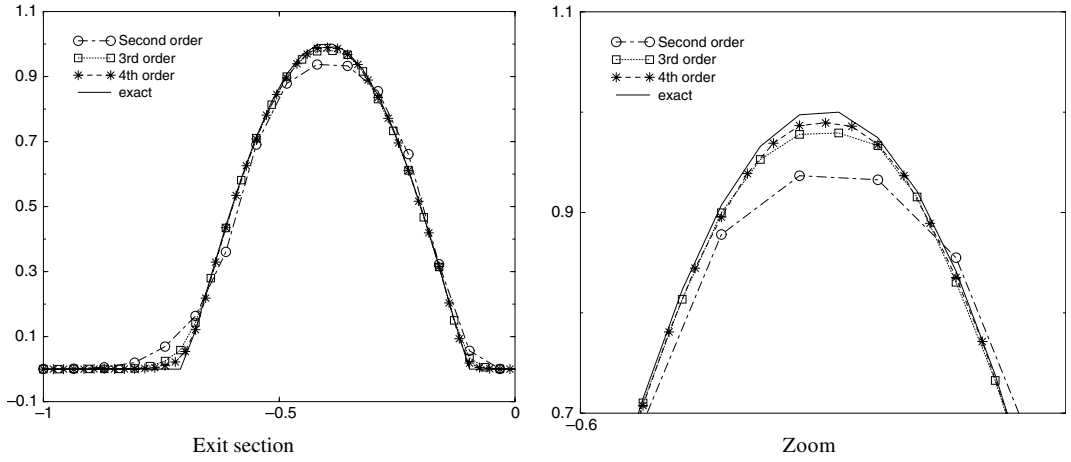

Fig. 34. Plot of the solutions in the interval $[-1,0]$, and zoom around the maximum.

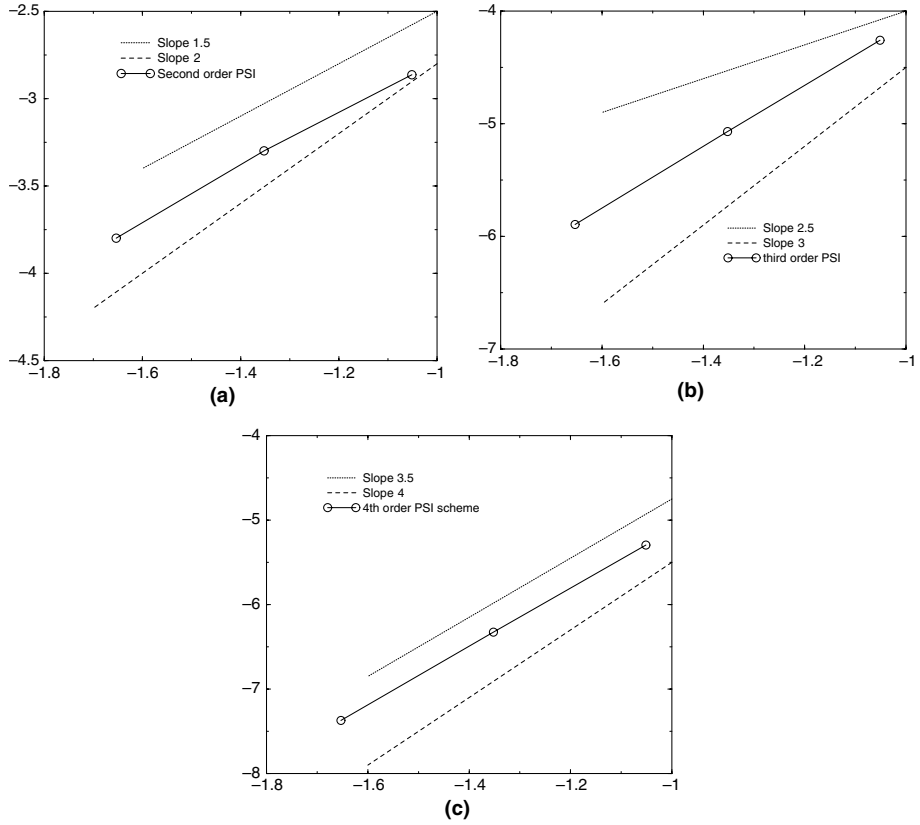

Fig. 35. L^2 error of the (a) second order, (b) third order and (c) fourth order PSI schemes.

4.2.2. Burger equation

We consider the Burger equation

$$\frac{1}{2}\frac{\partial u^2}{\partial x}+\frac{\partial u}{\partial y}=0, \quad x\in[0,1]\times[0,1],$$

$u(x,y)=1.5-2x$ on the inflow boundary.

The exact solution is

$$u(x,y)=\begin{cases}-0.5 & \text{if } y\leqslant 0.5 \text{ and } -2\left(x-\frac{3}{4}\right)+y-\frac{1}{2}\leqslant 0,\\ 1.5 & \text{if } y\leqslant 0.5 \text{ and } -2\left(x-\frac{3}{4}\right)+y-\frac{1}{2}\geqslant 0,\\ \max\left(-0.5,\min\left(1.5,\frac{x-\frac{3}{4}}{y-\frac{1}{2}}\right)\right) & \text{else.}\end{cases}$$

Once more, the solution is computed with a pseudo-time marching algorithm, the initial condition is set to $u=-0.5$. We represent the solutions computed for the

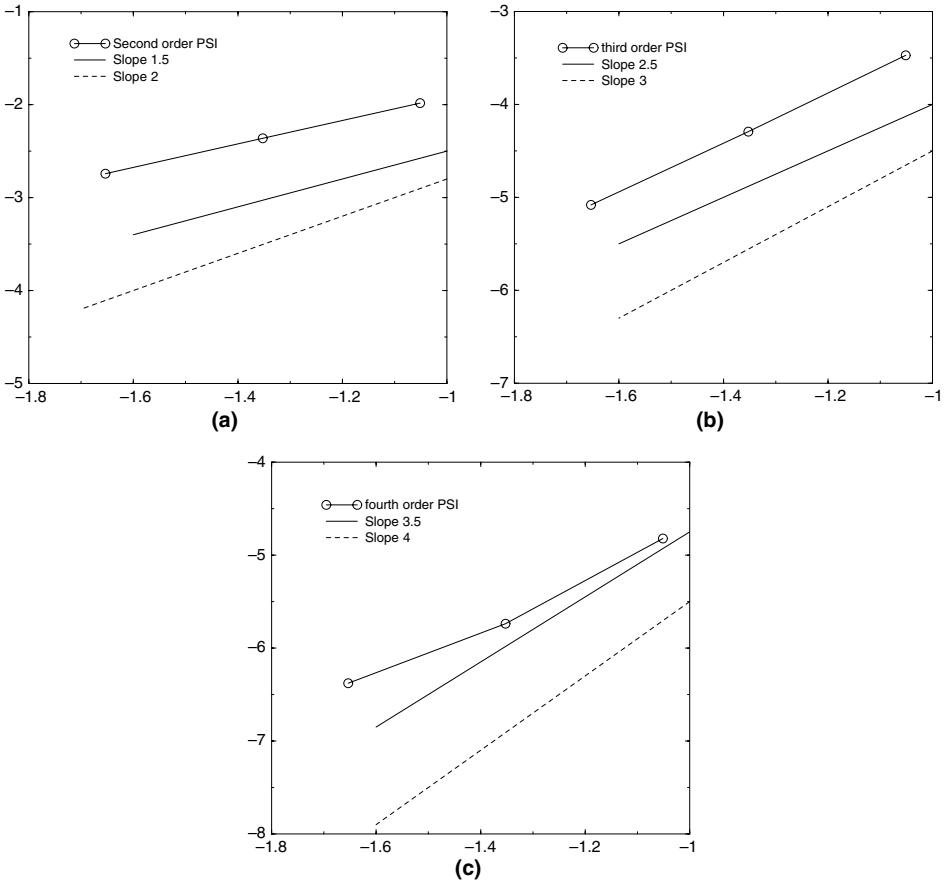

Fig. 36. L^{∞} error of the (a) second order, (b) third order and (c) fourth order PSI schemes.

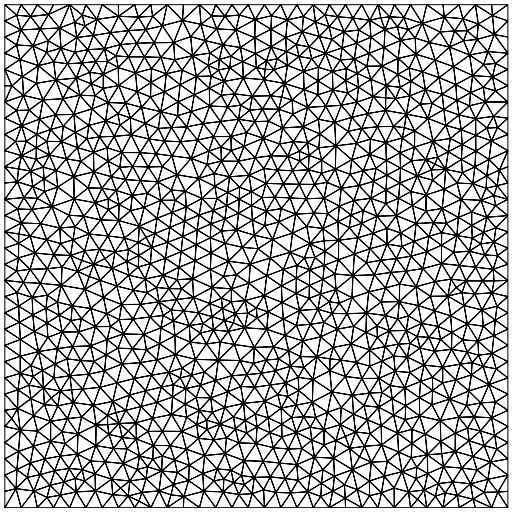

Fig. 37. Mesh for the Burger's equation.

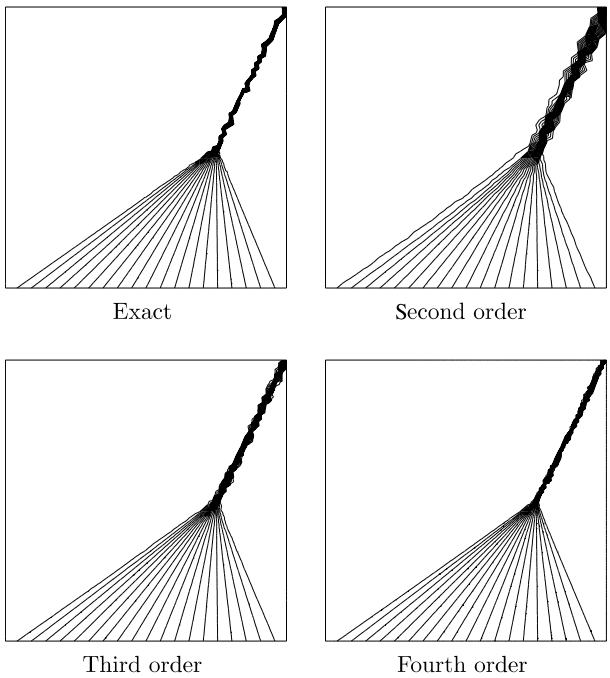

Fig. 38. Isolines of the exact and computed solutions, Burger's problem.

mesh represented in Fig. 37 with 1041 vertices and 1960 triangles.

The isolines of the solutions are displayed in Fig. 38. We also display cross-sections for $y = 0.75$ across the discontinuity (Fig. 39) and $y = 0.25$ across the fan (Fig. 40).

Last, we give a zoom of the cross-section $y = 0.25$ around the corner of the fan in Fig. 41. We see a very clear improvement of the quality of the solution with the increase of the accuracy order.

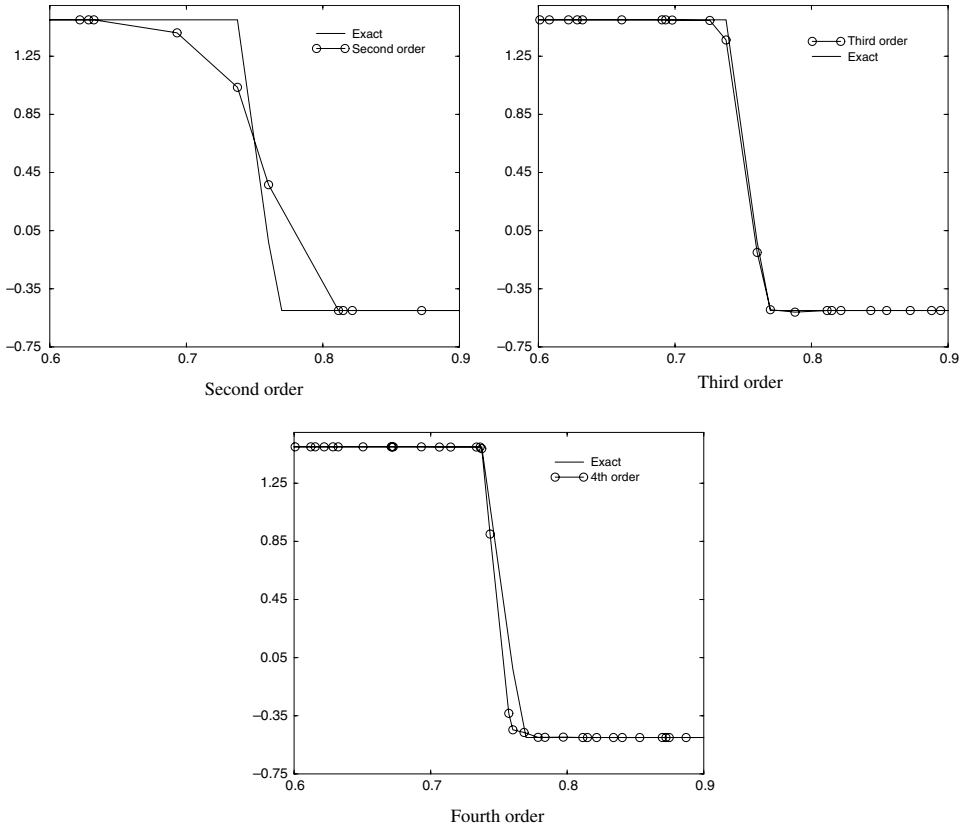

Fig. 39. Plot of the solutions across the shock, $y = 0.75$.

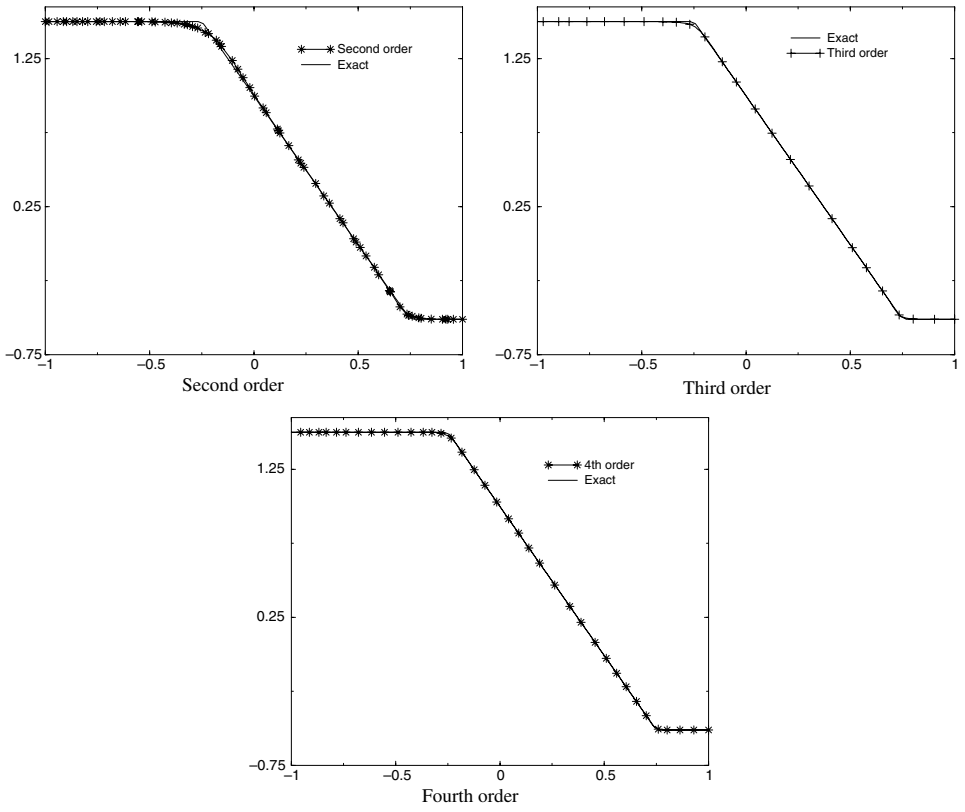

Fig. 40. Plot of the solutions across the fan, $y = 0.25$.

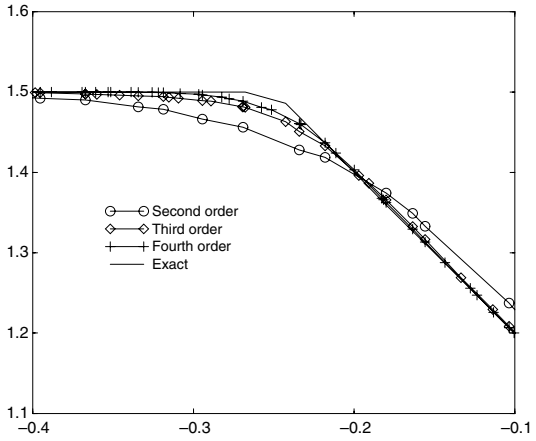

Fig. 41. Zoom across the fan, around the corner.

5. Conclusion

In this paper, we have tried to provide an exhaustive description of the state-of-the art of residual distribution schemes for the Euler equations of a calorically perfect gaz. Several issues have not been covered, for example the case of more general systems, such as the MHD system (see [30] for details), the problem of linearisation for non-polytropic gases (see [30]). Very few details on viscous problems have been given.

The main issues now, besides a better theoretical understanding of these schemes, including the problems and partial solution described in Section 4, to construct efficient schemes for unsteady problems with higher than second order accuracy. A first version has been described in [22], a better one in [51], but the situation is far from being satisfactory. Another issue is to understand how this type of methodology can be extended to nonconformal meshes.

Acknowledgements

We would like to thank Herman Deconinck (VKI), Mario Ricchiutto (VKI and now INRIA), Mohamed Mezine (Numeca), Nikolai Andrianov (Bordeaux), Michel Ravachol (Dassault), P.L. Roe (Ann Harbor) for many stimulating discussions. The financial support of the French Atomic Commission (CEA) through the LRC-M03 grant is also acknowledged, as well as the support of the french ministry of Research through the Supersonic Transport Program (Décision 02 T 0313, October 8th 2002). This work has also supported in part by E.U. RT Network Hyke HPRN-CT-2002-0282. Boniface Nkonga (Bordeaux and INRIA) is also thanked: the numerical illustrations have all been done using the platform `Fluid-Box` that he has written. Last, Mohamed Hafez (UC Davis) is warmly thanked for having suggested this paper and his patience.

Appendix A. Stability of Ricchiuto's variant of the N scheme

In this analysis, we assume a compactly supported solution. Starting from the N scheme (37), (39), we rewrite it as

$$|C_i|u_i^{n+1} + \sum_{j\neq i} c_{ij}(u_i^{n+1} - u_j^{n+1}) = |C_i|u_i^n$$

with

$$c_{ij} = \sum_{T\ni i} c_{ij}^{\mathrm{T}}$$

and

$$c_{ij}^{\mathrm{T}} = \Delta t k_i^+ n k_j^-.$$

Here $|C_i| = \sum_{T\ni i} \frac{|T|}{3}$ is the area of the dual cell.

A.1. L^∞ stability

The scheme writes $Au^{n+1} = u^n$ with

$$a_{ii} = 1 + \sum_j \frac{c_{ij}}{|C_i|} > 0 \quad \text{if } j = i,$$

$$a_{ij} = -\frac{c_{ij}}{|C_i|} < 0 \quad \text{if } i \neq j,$$

so that A^{-1} is a matrix with positive entries. This guaranties the maximum principle.

A.2. Energy analysis

After multiplication by u_i^{n+1} and summation, we get

$$\mathscr{E}^{n+1} + \sum_i \sum_j c_{ij}(u_i^{n+1} - u_j^{n+1})u_i^{n+1} = \sum_i |C_i|u_i^n u_{i+1}^{n+1},$$

where

$$\mathscr{E}^{n+1} = \sum_u |C_i|(u_i^{n+1})^2.$$

Then we rearrange the second term,

$$\sum_i \sum_j c_{ij}(u_i^{n+1} - u_j^{n+1})u_i^{n+1} = \sum_T \sum_{i,j\in T} c_{ij}^{\mathrm{T}}(u_i^{n+1} - u_j^{n+1})u_i^{n+1}.$$

The second summation

$$\sum_{i,j\in T} c_{ij}(u_i^{n+1} - u_j^{n+1})u_i^{n+1}$$

can be rewritten as

$$1/2\sum_j k_j(u_j^{n+1})^2 + 1/2\sum_{i,j\in T} c_{ij}^{\mathrm{T}}(u_i^{n+1} - u_j^{n+1})^2$$

because we have the relations $\sum_{j\neq i}(c_{ij}^{\mathrm{T}} - c_{ji}^{\mathrm{T}}) = k_i$. Coming back to the problem, we have

$$2\mathscr{E}^{n+1} + \sum_T \sum_j k_j^{\mathrm{T}}(u_j^{n+1})^2 + \sum_{i,j} c_{ij}(u_i^{n+1} - u_j^{n+1})^2 = 2\sum_i |C_i|u_i^{n+1}u_i^n.$$

Assuming now a *constant* velocity field, the second sum vanishes and we get

$$\mathscr{E}^{n+1} \leqslant \sum_i |C_i| u_i^{n+1} u_i^n \leqslant 1/2(\mathscr{E}^{n+1} + \mathscr{E}^n)$$

so that

$$\mathscr{E}^{n+1} \leqslant \mathscr{E}^n$$

unconditionally on Δt.

References

[1] Harten A. On the symmetric form of conservation laws with entropy. J Comput Phys 1983;49:151–64.

[2] Tadmor E. The numerical viscosity of entropy stable schemes for systems of conservation laws. Math Comput 1987;49:91–103.

[3] Hussaini MY, van Leer B, van Rosendal J, editors. Upwind and high resolution schemes. Springer-Verlag; 1997.

[4] Struijs R, Deconinck H, Roe PL. Fluctuation splitting schemes for the 2D Euler equations. VKI LS 1991-01. Computational fluid dynamics, 1991.

[5] Deconinck H, Struijs R, Bourgeois G, Roe PL. Compact advection schemes on unstructured meshes. VKI Lecture Series 1993-04. Computational fluid dynamics, 1993.

[6] Ni R-H. A multiple grid scheme for solving the Euler equations. AIAA J 1981;20:1565–71.

[7] Lerat A, Corre Ch. A residual-based compact scheme for the compressible Navier–Stokes equations. J Comput Phys 2001;170(2): 642–75.

[8] Lerat A, Corre Ch. Residual-based compact schemes for multidimensional hyperbolic systems of conservation laws. Comput Fluids 2002;31(4–7):639–61.

[9] Corre C, Hanss G, Lerat A. A residual-based compact scheme for the unsteady compressible Navier-Stokes equations. Comput Fluids 2005;34(4–5):561–80.

[10] Roe PL. Characteristic-based schemes for the Euler equations. Ann Rev Fluid Mech 1986;18:337–65.

[11] Paillre H. Multidimensional upwind residual discretisation schemes for the Euler and Navier Stokes equations on unstructured meshes. PhD thesis, Universit Libre de Bruxelles, 1995.

[12] van der Weide E. Compressible flow simulation on unstructured grids using multi-dimensional upwind schemes. PhD thesis, Delft University of Technology, Netherlands, 1998.

[13] Deconinck H, Sermeus K, Abgrall R. Status of multidimensional upwind residual distribution schemes and applications in aeronautics. AIAA paper 2000-2328, June 2000. AIAA CFD Conference, Denver, USA.

[14] Abgrall R. Toward the ultimate conservative scheme: following the quest. J Comput Phys 2001;167(2):277–315.

[15] Abgrall R, Barth TJ. Weighted residual distribution schemes for conservation laws via adaptive quadrature. SIAM J Sci Comput 2002;24(3):732–69.

[16] Abgrall R, Mezine M. A consistent upwind residual scheme for scalar unsteady advection problems. In: Conference AMIF organized by the European Science Foundation, Tuscany, Italy, October 2000.

[17] Abgrall R, Mezine M. Construction of second order accurate monotone and stable residual distribution schemes for steady problems. J Comput Phys 2004;195(1):474–507.

[18] Abgrall R, Mezine M. Construction of second order accurate monotone and stable residual distribution schemes for unsteady flow problems. J Comput Phys 2003;188(1):16–55.

[19] Abgrall R, Deconinck H. Residual Distribution Schemes, discontinuous Galerkin schemes and mesh adaptation. Comput Fluids 2005;34(4–5):561–80.

[20] Abgrall R, Mezine M. Residual distribution schemes for steady problems. In: von Kàrman Institute Lecture Series, March 2003.

[21] Mezine M, Ricchiuto M, Abgrall R, Deconinck H. Monotone and stable residual distribution schemes on prismatic space–time elements for unsteady conservation laws. In: von Kàrman Institute Lecture Series, March 2003.

[22] Ricchiuto M, Abgrall R, Deconinck H. Very high order fluctuation splitting schemes for unsteady scalar advection. In: von Kàrman Institute Lecture Series, March 2003.

[23] Deconinck H, Roe PL, Struijs R. A multidimensional generalisation of Roe's difference splitter for the Euler equations. Comput Fluids 1993;22(2/3):215–22.

[24] van der Weide E, Deconinck H. Positive matrix distribution schemes for hyperbolic systems. In: Désidéri, Hirch, Le Tallec, Pandolfi, Périaux, editors. Computational fluid dynamics '96. Wiley; 1996. p. 747–53.

[25] Barth TJ. Some working notes on the N scheme. Private communication, 1997.

[26] Deconinck H, Struijs R, Bourgeois G, Roe PL. Compact advection schemes on unstructured meshes. VKI Lecture Series 1993-04, Computational fluid dynamics, 1993.

[27] Abgrall R, Mer K, Nkonga B. A Lax–Wendroff type theorem for residual schemes. In: Hafez M, Chattot JJ, editors. Innovative methods for numerical solutions of partial differential equations. World Scientific; 2002. p. 243–66.

[28] Abgrall R. On essentially non-oscillatory schemes on unstructured meshes: analysis and implementation. J Comput Phys 1994;114(1): 45–54.

[29] Abgrall R. Approximation du problème de Riemann vraiment multidimensionnel des équations d'Euler par une méthode de type Roe (I): la linéarisation. C R Acad Sci I Math 1994;319:499–504.

[30] Csík A, Ricchiuto M, Deconinck H. A conservative formulation of the multidimensional upwind residual distribution schemes for general nonlinear conservation laws. J Comput Phys 2002;179(1): 286–312.

[31] Lax P, Wendroff B. Systems of conservation laws. Commun Pure Appl Math 1960;13:217–37.

[32] Kröner D, Rokyta M, Wierse M. A Lax–Wendroff type theorem for upwind finite volume schemes in 2-d. East-West J Numer Math 1996;4(4):279–92.

[33] Johnson C, Nävert U, Pitkäranta J. Finite element methods for linear hyperbolic problems. Comput Methods Appl Mech Eng 1984;45(1–3):285–312.

[34] Hughes ThJR, Mallet M, Mizukami A. A new finite element formulation for computational fluid dynamics: II Beyong SUPG. Comput Methods Appl Mech Eng 1986;54:341–55.

[35] Abgrall R, Roe PL. Construction of very high order fluctuation scheme. J Sci Comput 2003;19(1–3):3–36.

[36] Breuss M. The correct use of the Lax-Friedrichs method. 2004.

[37] Deconinck H, Sermeus K, Abgrall R. Status of multidimensional upwind residual distribution schemes and applications in aeronautics. AIIA paper 2000-2328, June 2000.

[38] Henriques JCC, Gato LMC. A multi-dimensional upwind matrix distribution scheme for conservation laws. Comput Fluids 2004;33(5–6):755–70.

[39] Abgrall R. Essentially non oscillatory residual distribution schemes for hyperbolic problems. J Comput Phys, in press.

[40] Csik A , Ricchiuto M, Deconinck H, Poedts S. Space–time residual distribution schemes for hyperbolic conservation laws. AIAA Paper 2001–2617, 2001.

[41] Csik A. Upwind residual distributive schemes of general hyperbolic conservation laws and applications to ideal MHD. PhD thesis, Leuwen, Belgium, 2001.

[42] Mezine M. Conception de schémas vraiment multidimensionnels pour les écoulements compressibles instationnaires. PhD thesis, Mathématiques Appliquées, Université Bordeaux I, December 2002.

[43] Collela P, Woodward P. The numerical simulation of two-dimensional fluid with strong shocks. J Comput Phys 1984;54:115–73.

[44] Quirk JJ. A contribution to the great Riemann solver debate. Int J Numer Methods Fluids 1994;18:555–74.
[45] Ben-Dor G. Shock wave reflection phenomena. Berlin/New York: Springer–Verlag; 1991.
[46] Pao SP, Salas MD. AIAA Paper 81-1205, 1981.
[47] Meadows KR, Kumar A, Hussaini MY. A computational study of the interaction between a vortex and a shock wave. AIAA Paper 89-1043, 1989.
[48] Jiang G-S, Shu C-W. Efficient implementation of weighted eno schemes. J Comput Phys 1996;126:202–28.
[49] Dobes J, Ricchiuto M, Deconinck H. Implicit space–time residual distribution method for unsteady laminar viscous flow. Comput Fluids 2005;34(4–5):593–615.
[50] Yee HC, Sandham ND, Djomehri MJ. Low-dissipative high-order shock-capturing methods using characteristic-based filters. J Comput Phys 1999;150:199–238.
[51] Abgrall R, Andrianov N, Mezine M. Towards very high-order accurate schemes for unsteady convection problems on unstructured meshes. Int J Numer Methods Fluids 2005;47(8–9):679–91.